LITHOS 488-489 (2024) 107797

Contents lists available at ScienceDirect

LITHOS

journal homepage: www.elsevier.com/locate/lithos

Research Article

# Rheology modification in a subduction channel due to eclogite facies metasomatism (Rocky Beach Metamorphic Mélange, Port Macquarie, Australia)

M.A. Finch [a,b,c,*], A. Olesch-Byrne [a,b,c], T. Chapman [d], M. Beilharz [c], A.G. Tomkins [c]

[a] The University of Melbourne, School of Geography, Earth and Atmospheric Sciences, Parkville, Victoria, Australia
[b] James Cook University, Earth and Environmental Science, Townsville, Queensland, Australia
[c] Monash University, School of Earth, Atmosphere and Environment, Clayton, Victoria, Australia
[d] University of New England, Earth Science, School of Environmental and Rural Science, Armidale, New South Wales, Australia

ARTICLE INFO

*Keywords:*
Subduction channel
Rheology
High pressure metasomatism
Mélange

ABSTRACT

The rheological properties of the interface between the down-going and overriding plates in subduction zones provides insight into how plate convergence is accommodated and the controls on seismic and aseismic slip. This interface is known as the subduction channel and exhumed examples provide the only direct information on deformation mechanisms and the impact of metamorphism on rheology. The Rocky Beach Metamorphic Mélange in eastern Australia is one such exhumed subduction channel, composed of eclogite, blueschist and greenschist facies blocks within a mélange matrix. Previous phase equilibria modelling indicates that high pressure blocks were subducted to ca. 100 km depth and then retrogressed during return flow and exhumation. We found that the rheology of blocks is modified by metasomatism, consistent with studies on other subduction channels. However, through comparison of blocks from different metamorphic grades we found that the effect of metasomatism on rheology varied depending on the pressure and temperature conditions of metasomatism. While unmetasomatised eclogites behaved as rigid objects in the mélange matrix, rocks with mineral assemblages that equilibrated during eclogite facies metasomatism accumulated significant strain, forming isoclinal folds and refolded folds. Deformation of these blocks began at eclogite facies and continued during return flow and retrogression to blueschist facies. At blueschist facies, metasomatised blocks developed mm-scale isoclinal folds with shearing parallel to fold limbs forming rootless isoclinal folds. At the transition between blueschist and greenschist facies, pressure solution became important, preferentially focusing along layers of lawsonite, dissolving it from the rock. At greenschist facies, dissolution-precipitation processes caused significant mass loss, producing mm-spacing between pressure solution seams and cuspate folds, analogous to dewatering structures in sediments. In the Rocky Beach Metamorphic Mélange eclogite facies metasomatism reduces the competence of rigid blocks, reducing overall subduction channel heterogeneity during return flow. We suggest that subduction channels that experience widespread eclogite facies metasomatism may be less likely to generate seismic slip during return flow, since the proportion of rigid blocks and block strength are both reduced.

## 1. Introduction

Subduction channels form at the interface between the down-going slab and the overriding plate and are zones of intense deformation hundreds to thousands of metres thick (Agard et al., 2018; Cloos and Shreve, 1988a). Exhumed examples at blueschist to eclogite facies are either continuous slices or mélanges with a block-in-matrix structure, where rigid blocks are high pressure, low temperature metamorphic rocks with a peridotite, basaltic or sedimentary protolith. A low viscosity, highly-strained mélange matrix surrounds these blocks and is a hybrid of the three block types, generated through physical and chemical mixing (Cloos, 1982; Festa et al., 2010). Subduction channels accommodate most of the deformation during active subduction (Cloos and Shreve, 1988b) and their rheology controls seismic and aseismic slip (e.g., Fagereng and Sibson, 2010; Penniston-Dorland and Harvey, 2023; Platt et al., 2018; Tichelaar and Ruff, 1993).

* Corresponding author at: The University of Melbourne, School of Geography, Earth and Atmospheric Sciences, Parkville, Victoria, Australia.
*E-mail address:* melanie.finch@unimelb.edu.au (M.A. Finch).

https://doi.org/10.1016/j.lithos.2024.107797
Received 10 November 2023; Received in revised form 8 August 2024; Accepted 5 September 2024
Available online 7 September 2024

Previous work on the rheology of subduction channel melanges has determined that high viscosity contrasts between the weak mélange matrix and rigid blocks causes strong strain localisation. This typically leaves the blocks only weakly deformed, to the extent that many exhumed examples preserve magmatic textures of the protolith (e.g., Gao and Klemd, 2003; Stöckhert, 2002; Stöckhert and Renner, 1998). In these settings blocks behave rigidly and the primary control on subduction channel rheology is the mélange matrix and interactions between blocks (Beall et al., 2019a; Grigull et al., 2012). Conversely, some subduction channels contain deformed high P blocks (McNamara et al., 2024), which are inferred to have accumulated strain during discrete episodes along the P-T path where a transient set of conditions caused temporary strain localisation to the block (Wassmann and Stöckhert, 2013).

Block rheology can change as subduction progresses due to metamorphism-induced mineralogical changes (e.g., Behr and Platt, 2013) including metasomatism, where metamorphism occurs in the presence of a chemically-reactive fluid that causes alteration to the parent rock involving simultaneous reactions and changes in bulk rock composition (Goncalves et al., 2013). Mineralogical changes during prograde metamorphism can strengthen the subduction channel shear zone if newly formed minerals are stiffer than their precursors, such as when amphibolite facies minerals (e.g., amphibole and pyroxene) replace the weaker sheet silicates stable at lower metamorphic grade (Gyomlai et al., 2021; Penniston-Dorland et al., 2018). Conversely, metamorphism may lead to the replacement of stronger minerals by weaker ones, as is the case when metasomatism of ultramafic blocks produces talc or serpentine, which are common constituents of subduction channels (Peacock and Hyndman, 1999). Physical and chemical mixing in subduction systems makes rheological changes harder to predict because these processes produce rocks that are not seen in any other tectonic setting, including jadeitites, omphacitites, and 'blackwalls', which are chemical hybrids between serpentinite mélange matrix and mafic blocks (Marschall and Schumacher, 2012). The only way to understand how these peculiar rock assemblages form, interact and affect rheology to is study exhumed examples.

To understand rheological changes during metasomatism we focus here on the Rocky Beach Metamorphic Mélange (RBMM), which is a subduction channel that preserves blocks with unusual bulk compositions including omphacitites, lawsonite-blueschist 'conglomerates' and eclogite-facies rocks dominated by phengite and titanite (Och et al., 2003; Tamblyn et al., 2020a; Tamblyn et al., 2020b), as well as some of the highest pressure lawsonite-bearing rocks known worldwide (Whitney et al., 2020). The RBMM also includes mafic blocks that have been metasomatized at greenschist, blueschist or eclogite facies, affording the opportunity to examine how metasomatism changes rheology and deformation style from high to low pressure, which is the focus of this study.

## 2. Geologic setting

The Rocky Beach Metamorphic Mélange occurs within the Port Macquarie Serpentinite Mélange, which is part of the New England Orogen (NEO) in Eastern Australia (Fig. 1). The NEO is the youngest section of the Tasmanides, which are a series of orogens that progressively grew the eastern margin of Gondwana from the Cambrian to the Triassic (Leitch, 1974; Phillips and Offler, 2011). This sequence started with the Delamerian Orogen at 515–490 Ma and the Lachlan-Thompson Orogen at 484–375 Ma (Glen, 2005; Jessop et al., 2019; Kemp et al., 2009). The transition from the Lachlan-Thompson orogen to the NEO occurred at ca. 375 Ma and was followed by a number of cycles of extension and compression, with the final extensional period ending at ca. 200 Ma (Jessop et al., 2019). The NEO contains arc, forearc and accretionary complex rocks (Jessop et al., 2019). To the south, the forearc (Tamworth Belt) and accretionary complex (Tablelands complex) rocks are separated by the Peel-Manning Fault System, which is a

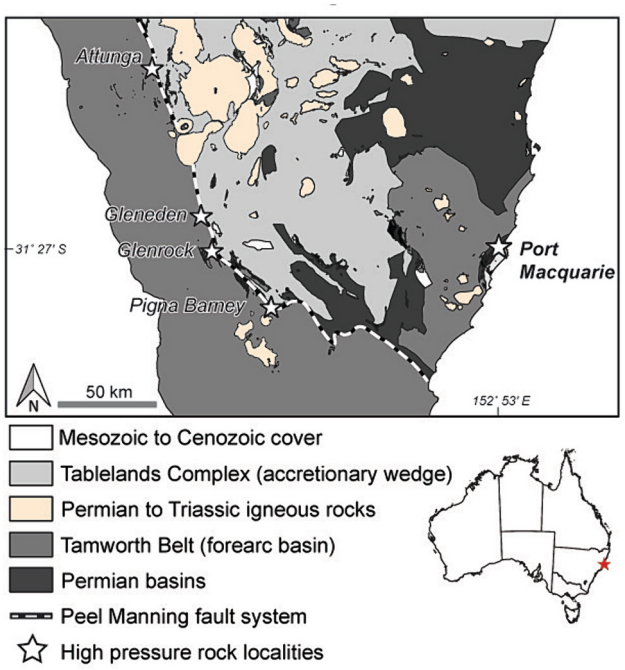


**Fig. 1.** Regional map showing major lithologies, high pressure rock localities on the Peel Manning Fault System and the location of Port Macquarie. The South New England Orogen includes the arc, forearc (Tamworth Belt) and accretionary complex (Tablelands Complex) of the 375–200 Ma orogenic event.

serpentinite belt that contains a number of high P/low T blocks that are Cambrian to Ordovician in age (Fig. 1; Leitch, 1974). These are thought to have formed in a subduction zone and were exhumed during eastward-directed slab rollback during the Permian to Triassic, emplacing them within the southern NEO (Allan and Leitch, 1992; Leitch, 1974; Manton et al., 2017; Phillips et al., 2015; Phillips and Offler, 2011). Although the Port Macquarie Serpentinite Mélange is not contiguous with the Peel-Manning Fault System (Fig. 1), it encases similar rocks of the same age, indicating they were sourced from the same Delamerian subduction channel.

The Port Macquarie Serpentinite Mélange consists of eight outcrops of serpentinite that occur along the coast near the town of Port Macquarie (Och et al., 2007). The mélange contains a serpentinite matrix that hosts an assortment of blocks with subduction affinities, including accretionary complex, island-arc, and high P/low T metamorphic rocks (Barron et al., 1976; Buckman et al., 2015; Och et al., 2003). The blocks are Cambrian to Devonian in age, whereas the final stages of movement in the encapsulating serpentinite have been dated to the Triassic at prehnite-pumpellyite facies (247 ± 20 Ma; Buckman et al., 2015; Och et al., 2003; Tamblyn et al., 2020a). One of the block types within the serpentinite is the Watonga Formation, which includes basalt, chert and volcaniclastic rocks that originally formed in a deep marine setting that were subsequently off-scraped during subduction and incorporated into the accretionary complex of the southern NEO, where rocks that span ages of 455 to <330 Ma were juxtaposed (Buckman et al., 2015). A block of Watonga Formation is included within the Rocky Beach Metamorphic Mélange at the northern end of Rocky Beach which in turn is encased in the Port Macquarie Serpentinite Mélange.

The RBMM outcrops along a 150 m stretch of coast line (Figs. 1, 2) and consists of high P/low T blocks within a mélange matrix that varies in composition from mafic to ultramafic (Barron et al., 1976; Och et al., 2003). Most high P/low T blocks are blueschist-eclogite facies mafic rocks that have been variably affected by metasomatism, described in Sections 4 and 5. Blocks with other protoliths include marble, peridotites, pyroxenites and chert, and are not the focus of this study (Fig. 2).

Dating of the mafic blocks indicates that peak metamorphism

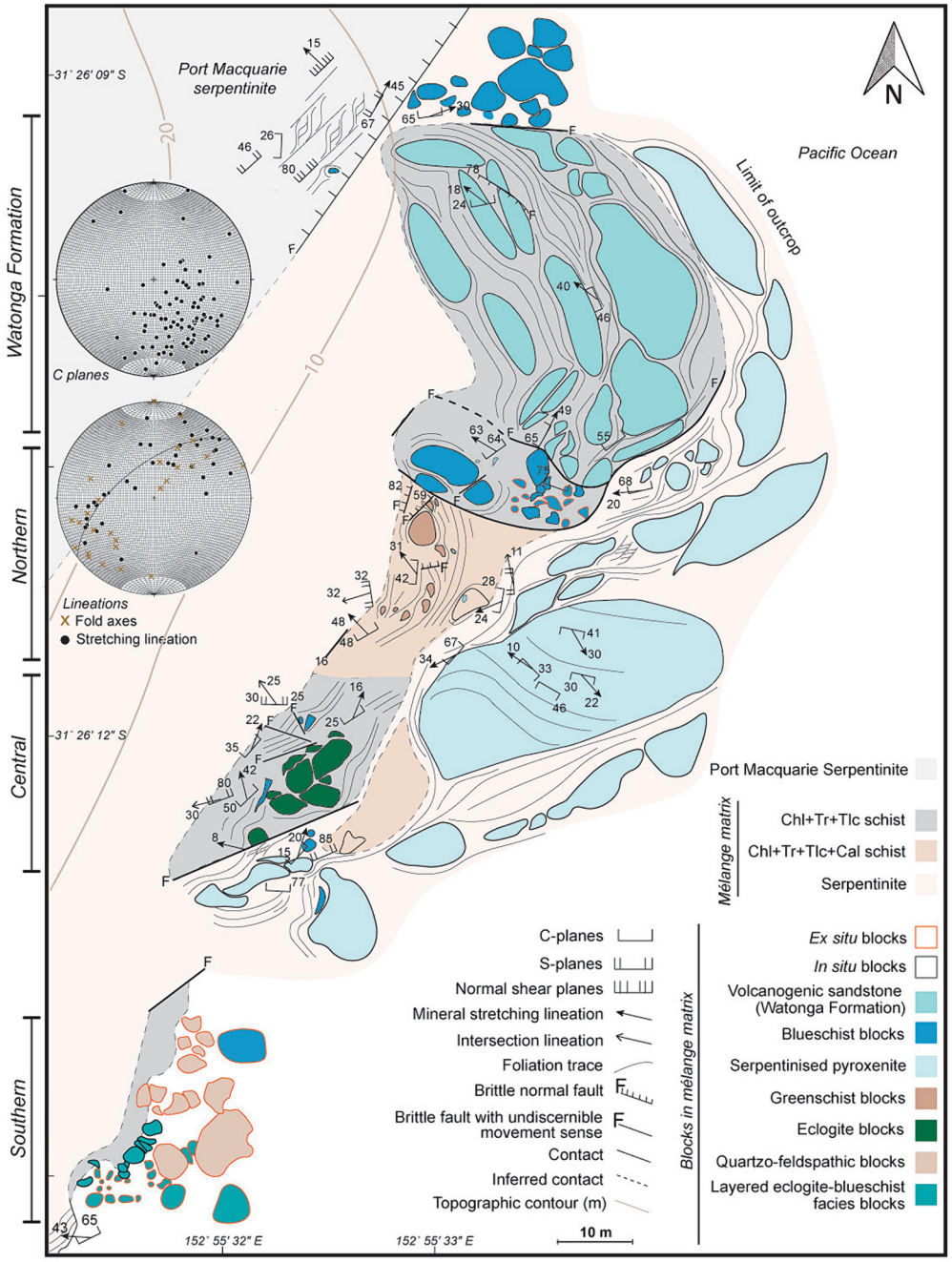


**Fig. 2.** Geological map of the Rocky Beach Metamorphic Mélange. Inset: Stereographic projection of C planes, stretching lineations and fold axes. Blocks in the southern section are ex situ on the beach in the intertidal zone.

occurred during the Late Cambrian to Early Ordovician (Och et al., 2003; Tamblyn et al., 2020a; Tamblyn et al., 2020b). Tamblyn et al. (2020a) dated garnet and lawsonite using Lu—Hf and Sm—Nd in a garnet blueschist and an eclogite facies rock from the RBMM. They found that the eclogite had a whole rock-garnet-lawsonite isochron age of 487 ± 11 Ma and the blueschist had a garnet – whole rock age of 472 ± 2 Ma. They interpreted that the difference in Lu—Hf ages was a result of later subduction of younger block, and subsequent juxtaposition of the two blocks in the mélange. This juxtaposition is thought to be due to 'return flow', where subducted material migrates into the serpentinised section of the overlying mantle wedge and flows up-dip along the subduction interface (Cloos, 1982; Cloos and Shreve, 1988a, 1988b). This process creates a mélange with an array of exotic blocks, sampled from different metamorphic grades and depths within the subduction zone (e.g., Krebs et al., 2008; Penniston-Dorland et al., 2018; Tamblyn et al., 2020b). In this model, subducting (down-going) rocks close to the interface with the upflowing section of the subduction channel are incorporated into the latter and transported upwards (Wassmann and Stöckhert, 2013). Thus, simply imagined, eclogites sampled deep in the system may be juxtaposed with blueschists and greenschists as the subduction channel shear zone incorporates new blocks at the same time as transporting blocks from deeper levels upwards.

Subsequent work by Tamblyn et al. (2020b) found that there were two generations of garnet in the eclogite facies rocks, which they attributed to two periods of prograde garnet growth due to cycling within the subduction channel as interpreted from geochronology, mineral zoning and phase equilibria modelling. In their model, rocks were first subducted to P/T of 29 kbar and 600 °C, after which they were

incorporated into the upgoing section of the subduction channel and partially exhumed during return flow, as indicated by dissolution textures in garnet and phase equilibria modelling. After this, rocks were purported to have been reincorporated into the down-going section of the subduction channel and reburied to a second peak at 27 kbar and 590 °C, before final exhumation before the Permian. They suggested that the Lu—Hf garnet dates (487 ± 11 Ma and 472 ± 2 Ma) represent the timing of the first stage of burial and garnet growth, since garnet cores are rich in Lu. They also dated titanite (U—Pb) and phengite (Ar—Ar and Rb—Sr) interpreted to have grown during reburial due to textural relationships including prograde zoning in phengite, which gave a reburial age of ca. 450 Ma.

We define the northern and southern limits of the RBMM as the contact between the Port Macquarie serpentinite and blueschists (northern contact), and between serpentinite and layered eclogite facies blocks (southern contact; Fig. 2). The contact to the west is covered by vegetation but we approximate its location from sparse outcrops revealed in eroded channels in the cliff face. The contact to the east is observable (discontinuously) on the beach at low tide. As previously mentioned, within the RBMM there is a block of Watonga Formation, indicating that deeply subducted rocks were juxtaposed against the accretionary prism prior to incorporation into the Port Macquarie serpentinite mélange.

## 3. Method

### 3.1. Microscopy techniques

Samples of the RBMM were studied and imaged using a petrographic microscope and further explored using a scanning electron microscope (JEOL 7001F FEG-SEM) at the Monash Centre for Electron Microscopy. Major and minor element mineral compositions were measured by microprobes at two laboratories (due to access limitations during the pandemic). At the Central Science Laboratory (University of Tasmania) a JEOL JXA-8530F Plus field emission electron microprobe was used. This microprobe was used for all quantitative mineral analyses except for those on Mac29 and Mac30a (Table S1). At the Advanced Characterisation Facility at the Commonwealth Scientific and Industrial Research Organisation (CSIRO) a JEOL 8530F was used. This microprobe was used to create all probe element maps and for quantitative mineral analysis of samples Mac29 and Mac30a (Table S1). Detail on the method is included in the supplementary methods.

To determine textural relationships of mineral phases, key thin sections were mounted on pure silica glass for analysis at the Australian Synchrotron (ANSTO, Clayton, Australia). The X-ray Fluorescence Beamline was used and element maps were collected with the Maia detector (Ryan et al., 2010). Detail on the method is included in the supplementary methods.

### 3.2. Phase equilibria modelling

Two bulk rock compositions were modelled for phase equilibria. The major element composition of a blueschist (PMRB1B) was determined from a crushed whole rock powder that was analysed by X-ray fluorescence (XRF) at ALS Global in Queensland, Australia. The major element bulk composition of a garnet-phengite schist was calculated by combining modal proportions of each mineral with its measured chemical composition (Fig. S1, Table 1). Thin sections were mapped at the Australian Synchrotron and element maps analysed using ImageJ to determine modal proportions. Mineral compositions were determined by microprobe, as detailed in the previous section.

Phase equilibria modelling was performed using THERMOCALC (Powell & Holland, 1988) in the NCKFMASHTO chemical system ($Na_2O$–CaO–$K_2O$–FeO–MgO–$Al_2O_3$–$SiO_2$–$H_2O$–$TiO_2$–O) using version 3.50 (Powell & Holland, 1988) and the internally consistent thermodynamic dataset 6.2 (updated 6th February 2012: Holland & Powell, 2011). Redox conditions were fixed at $Fe^{3+}/[Fe^{3+}+Fe^{2+}] = 0.15$ to match common ratios observed in MORB (Kelley & Cottrell, 2009) and a $H_2O$-H fluid ($H_2O$ activity = 0.99) fluid was modelled as in excess. Mn was not considered due to restricted partitioning in the activity–composition models, its absence should mostly influence the stability of garnet and chlorite (~50 °C; Chapman and Clarke, 2021). Biotite stability is overestimated in the models due to excess K and effectively low Al. The main phases that incorporate substantial K are muscovite and (less so) clinoamphibole. Additional phase equilibria calculations were completed with metastable biotite (e.g., White et al., 2004) to assess uncertainties on PT determinations. The absence of biotite results in a larger stability field of chlorite and narrower lawsonite–garnet transition to effectively accommodate Fe-Mg-Al exchange. The variance of individual isopleths between biotite-present and absent equilibria for garnet and omphacite is in the range of 2–50 °C and 1–2 kbar and for silica-in-phengite it is 10–50 °C and 2–3 kbar (Fig. S3). The variability is within predicted uncertainties of the method for determined PT estimates.

**Table 1**
Major element bulk rock compositions for the phase equilibria modelling in Fig. 9.

| Bulk | Blueschist | g–ph schist |
|---|---|---|
| $SiO_2$ | 44.25 | 44.33 |
| $Al_2O_3$ | 5.79 | 10.58 |
| CaO | 4.68 | 5.60 |
| MgO | 10.25 | 6.16 |
| FeO | 8.08 | 6.37 |
| $K_2O$ | 0.92 | 4.35 |
| $Na_2O$ | 4.33 | 0.75 |
| $TiO_2$ | 0.98 | 1.37 |
| O | 1.05 | 0.84 |
| $H_2O$ | 19.65 | 19.66 |

Mineral activity–composition models and abbreviations for phase equilibria modelling include: glaucophane (gl), actinolite (act), hornblende (hb), omphacite/diopside (o/dio: Green et al., 2016), feldspars (abc, pl: Holland et al., 2022), garnet (g), paragonite (pa), biotite (bi), muscovite (mu), chlorite (chl), chloritoid (ctd: White et al., 2014), epidote (ep), talc (ta: Holland & Powell, 2011). Phases treated as pure include lawsonite (law), rutile (ru), titanite (sph), quartz (q), coesite (coe), kyanite (ky) and $H_2O$-H (fluid). In the modelling the $H_2O$ fluid retains activities of >0.99.

## 4. Lithologies and structures

Although the RBMM consists of a range of lithologies including blocks of partially serpentinised peridotite, carbonate and silicified rocks (Fig. 2), the focus here is on metamorphic rocks that formed from mafic protoliths because these are more ammenable to petrological analysis and exert a strong influence on bulk composition and rheology of subduction systems globally. These are classified as eclogites, blueschists or greenschists based on their mineralogy, which reflects the bulk composition and the pressure and temperature of formation or re-equilibration. Three sections within the RBMM can be differentiated on the basis of mineralogy and structures within mafic blocks, as well as the composition of the mélange matrix: (1) the southern section, which contains layered eclogite-blueschist facies blocks, (2) the central section, which contains massive eclogites and blueschists, and (3) the northern section, which contains Lws-blueschists variably retrogressed to greenschist (Fig. 2). The mélange matrix consists of Tlc + Chl + Tr (mineral abbreviations after Whitney and Evans, 2010) with variable amounts of carbonate and serpentine.

Preliminary investigation of the Watonga Formation block encased in the RBMM revealed it consists of blocks of volcanogenic sandstone (Chl + Ab+San + Py) in a mélange matrix that consists mostly of chlorite, carbonate, chert and actinolite. Since the focus here is the

evolution of blocks with a mafic protolith, we do not discuss the Watonga Formation block in detail.

We describe the RBMM sections from south to north. Data from synchrotron element mapping and electron microprobe analysis of mineral compositions is incorporated in these descriptions and mineral compositions and end-member proportions are reported in Table S1.

### 4.1. Southern section

#### 4.1.1. Southern section lithologies

The southern section comprises blocks of layered eclogite-blueschist facies rock that have rounded to lens shapes up to 5 m in length (Fig. 3). Most of the blocks in this section are not in situ but found in the intertidal zone on the beach, eroded out of the densely vegetated cliff west of the beach. Although we found similar examples in situ, which occur in a matrix of Tlc + Chl + Tr, we focus on the ex situ examples as they provide an opportunity to understand the blocks in 3D. These ex situ blocks have been the focus of most of the previous work on the RBMM including Tamblyn et al. (2020a, 2020b) and Och et al. (2003).

Blocks in the southern section contain layers of (1) Omp + Grt ± Lws (eclogites), (2) Omp + Ttn ± Grt ± Ph ± Py (omphacitites), (3) Omp + Lws ± Ph ± Ttn (Lws-omphacitites), (4) Ph + Grt + Ttn + Lws + Py ± Omp (Grt-Ph schists), (5) Gln + Ph + Grt ± Ttn ± Ap (blueschists; Figs. 3, 4, 5, S1, S2). Some blocks show all layers with layer thicknesses from a few millimetres to tens of centimetres whereas other, smaller blocks are pure blueschist. Contacts between block layers are typically sharp, except for graditional contacts between omphacitite and blueschist layers in some blocks (e.g., Fig. 3d). In the layers of blueschist and Grt-Ph schist there is a foliation defined by the long axis of Gl and Ph respectively (Figs. 4, 5, S1, S2).

#### 4.1.2. Southern section structures

The large ex situ blocks (up to 5 m in diameter) commonly contain metre-scale fold hinges. Since these blocks are ex situ, the original orientation of structures cannot be determined, but they provide a rare opportunity for 3D observation and we see similar structures in nearby in situ blueschists in the southern and central sections (e.g., Fig. 6d). We focus here on two blocks at the northern end of Rocky Beach (Fig. 3a).

The first block we refer to as RB5; it is 4 m wide and consists of layers of Grt-blueschist, omphacitite, and Lws-omphacitite (Figs. 3a, 4c, 5c,e). These layers have been folded multiple times, with an isoclinal fold refolded by an isoclinal fold with a hinge perpendicular to the first generation, overprinted by 'upright' folding (relative geometry, block is not in situ). The overall shape of the block is sigmoidal (Fig. 3a), suggesting the block may have been a σ-type object within the mélange matrix when in situ, as seen with central section blocks described in the next section (e.g., Fig. 6d). In the limbs of the fold, layers of omphacitite have undergone brittle fracture and boudinage and glaucophane has filled the boudin necks (e.g., Figs. 4c, S2a). Some glaucophane-filled fractures are parallel to the axial plane of the 'upright' folding event (Fig. S1b).

The second block, RB1, consists of interlayered eclogite and Grt-blueschist. Layers are isoclinally folded and the block has a sigmoidal shape, similar to RB5. RB1 is variably retrogressed, with omphacitite fold limbs showing a gradual transition into blueschist (Fig. 3d). Garnet-phengite veins in the blueschist do not continue into the omphacite layer, but there are Grt + Ph veins filling fractures in the omphacite layer and along fold limbs. Below the isoclinally folded layer of omphacitite there are veins of pyrite that are folded and also appear as fine cross cutting veins that fan across the fold, perpendicular to the folded pyrite veins (Figs. 3b, S2b). These veins do not appear in the omphacitite layer, so presumably relate to fluid ingress during folding that affected only


**Fig. 3.** Ex situ blocks on the intertidal zone at Rocky Beach in the Southern Section. (a) Ex situ blocks eroded out of the cliff face. (b) Folded pyrite veins in block RB1 with pyrite veins perpendicular to layering and fanning across the fold (see inset in Fig. S2). (c) Folded interlayered blueschist and omphacitite-rich layer. (d) Relict omphacite-rich layers in fold hinges, interlayered with blueschist. White dashed lines highlight folds.

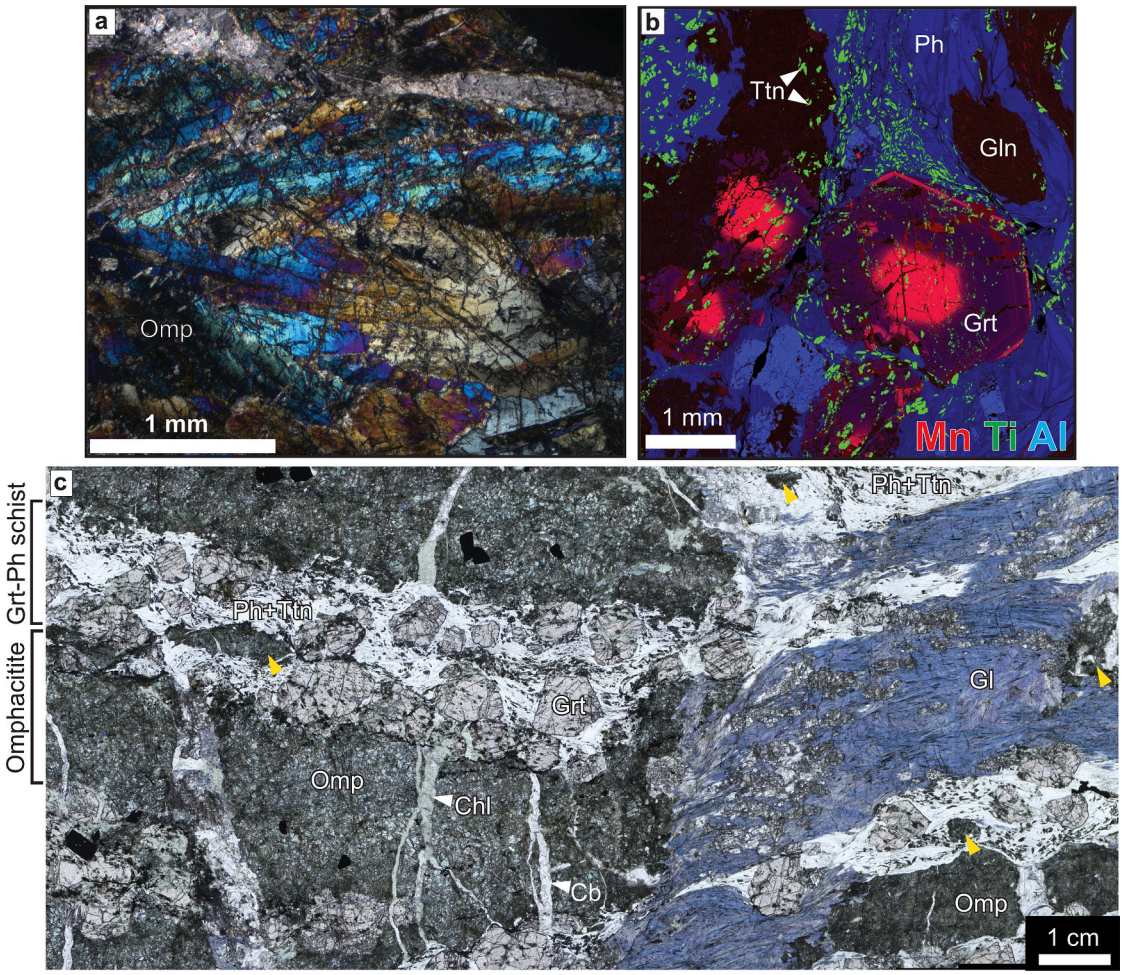


**Fig. 4.** Examples of mineral relationships from the southern section of the RBMM. (a) Microfolds in omphacite from an omphacitite (XPL). (b) Element map of manganese (red), titanium (green) and aluminium (blue) in a Grt-Ph schist. Titanite is included in Grt and is in the Grt-Ph matrix that wraps around Grt. (c) Layers of omphacitite, Grt-Ph schist and blueschist. Blueschist and Grt-Ph schist include pieces of omphacitite layer (yellow arrows) (PPL). (For interpretation of the references to colour in this figure legend, the reader is referred to the web version of this article.)

part of the block.

*4.1.3. Microstructures and mineral chemistry*

In the description of the major minerals below, the mineral features that the layers have in common are described before any unique attributes that appear only in one layer are noted. Layering is cross cut by carbonate veins (Figs. 3c, 4c) that contain rare phengite, glaucophane and titanite. Tamblyn et al. (2020a) determined that the carbonate in these veins is aragonite.

In thin section, omphacite is bright green in PPL and up to 3 mm in length with sweeping undulose extinction, poorly-formed kink bands and chlorite-filled pressure solution seams. In some samples omphacite shows crystal faces or forms tight folds on the sub-mm scale (Fig. 4a). In Lws-omphacitites, omphacite forms anhedral interlocking crystals around euhedral lawsonite (Fig. S2c,d). One sample, RB1C, contains a different appearance of omphacite, which is brown, anhedral and partially to completely replaced by chlorite. In this sample, omphacite contains inclusions of Ttn + Ph and phengite contains inclusions of Omp + Ttn. Microprobe analyses indicate that omphacite has proportions of diopside between 0.48 and 0.62, jadeite between 0.16 and 0.51, and aegirine between 0 and 0.31 (Table S1). One sample of Lws-omphacitite contained jadeite (0.91–0.96) in addition to omphacite (Table S1).

Garnet forms euhedral to subhedral porphyroblasts up to 5 mm diameter that contain inclusions of Ttn, Ap, Gln, Omp, Zrn, Qz, Stp, and Chl. Tamblyn et al. (2020a) also reported inclusions of Lws, Ph and Ep in garnet from similar samples. Inclusion trails of titanite and zircon in garnet are aligned with the external foliation and Ttn-rich layers also wrap around garnets (Fig. 4b). In Grt-Ph schists, garnet shows complex Mn and Y zoning, with oscillatory zoning and irregular Mn and Y zonation on garnet embayments (Fig. 5a). Similar zoning was previously described by Tamblyn et al. (2020b). This complex zoning is only in layers of Grt-Ph schist; it is absent from garnets in the other layers in southern section rocks, and from garnet in other sections. Garnets are partially retrogressed to chlorite, and in some blueschists they are pseudomorphed by chlorite. Microprobe analyses indicate garnet is $Alm_{38-69}Spss_{01-35}Grs_{23-37}Py_{0-11}$ with higher Spss and lower Alm and Py values in cores and zones with high Mn (Table S1).

Lawsonite forms euhedral crystals up to 5 mm long (Figs. 5b, S2c,d) and in Lws-Omphacitite layers, shows faint hourglass zoning in Sr, as well as more pronounced, irregular Sr zoning on porphyroblast rims (Fig. 5b). Rim zoning is discontinuous, typically appearing on just one or two sides of Lws grains and at the margins of Lws fractures and embayments (Fig. 5b). Lawsonite contains minor proportions of $TiO_2$ (up to 1 wt%) and FeO (up to 0.7 wt%; Table S1).

Phengite forms elongate grains up to 1 mm length parallel to the foliation (Figs. 4c, 5e, S2a) and also occurs as fine-grained aggregates in Lws-blueschists. At the margins between omphacitite/eclogite and Grt-Ph schist layers, phengite occasionally forms elongate blocky crystals that are oriented perpendicular to the contact (Fig. 5c,d). In some cases this texture is observed between two sections of an omphacitite or

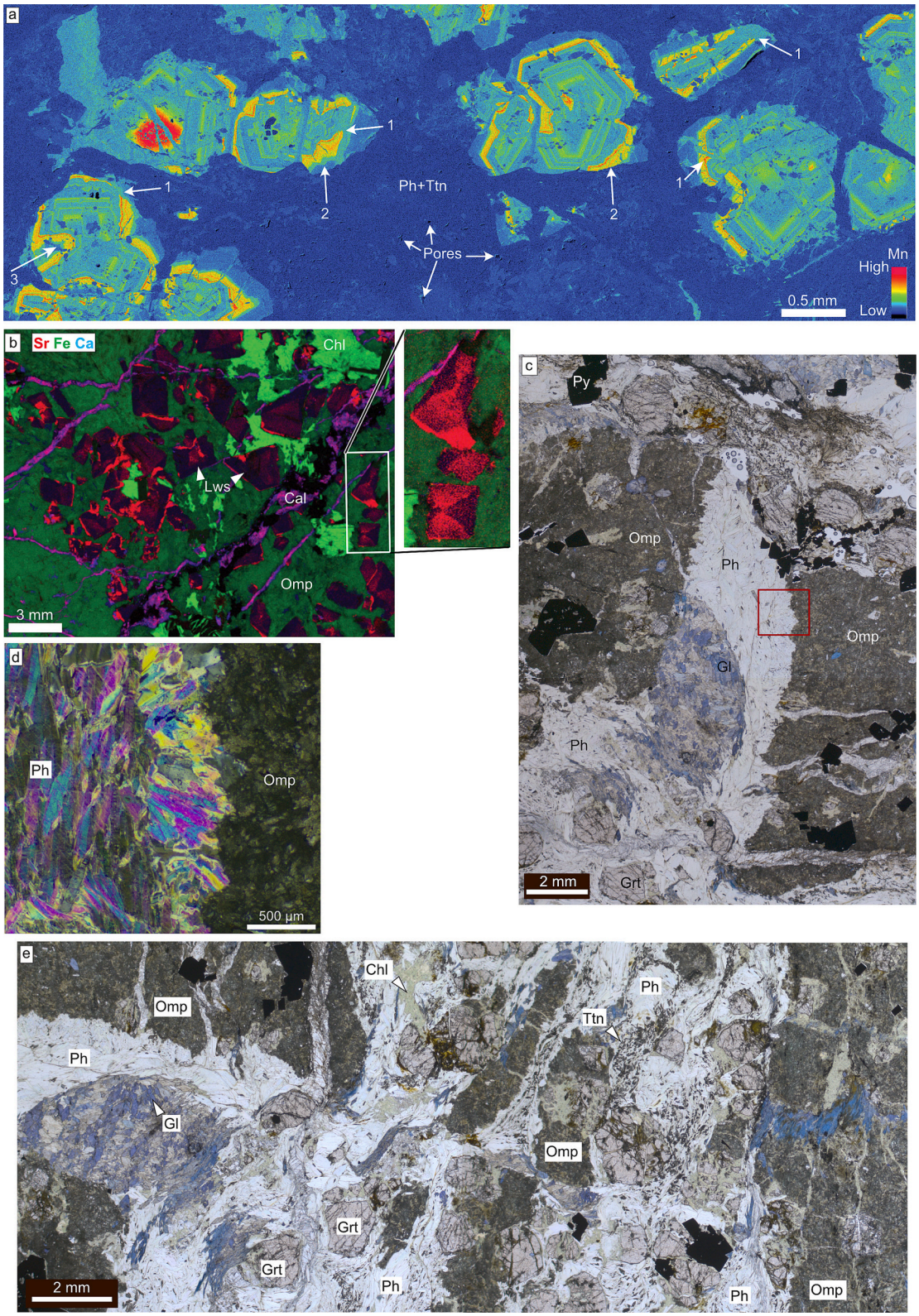


**Fig. 5.** Textures interpreted to indicate fluid-mediated growth of Grt-Ph schist layers. (a) Element map of Mn concentration showing oscillatory Mn zoning in garnet. The zones are truncated (arrows labelled 1), irregular (arrow labelled 2) and occur in embayments (arrow 3). The small black spots in the Ph-Ttn matrix are pores (labelled). (b) Element map of strontium (red), iron (green) and calcium (blue) of Lws-omphacitite. Lawsonite shows faint hourglass Sr zoning (white box with inset zoom) and more pronounced discontinuous Sr zoning on rims and in microfractures and embayments. (c) Photomicrograph of layers of Grt-Ph schist and omphacitite. The omphacitite layer has been fractured and a vein of Ph + Ttn has infilled the fracture. The area boxed in red is shown in (d) (PPL). (d) Photomicrograph of the wall of a Ph + Ttn vein with Ph oriented perpendicular to the vein wall (XPL). (e) Photomicrograph of layers of omphacitite and Grt-Ph schist. Pieces of the omphacitite layer have been fractured from the larger layers and incorporated in the Grt-Ph schist (PPL). (For interpretation of the references to colour in this figure legend, the reader is referred to the web version of this article.)

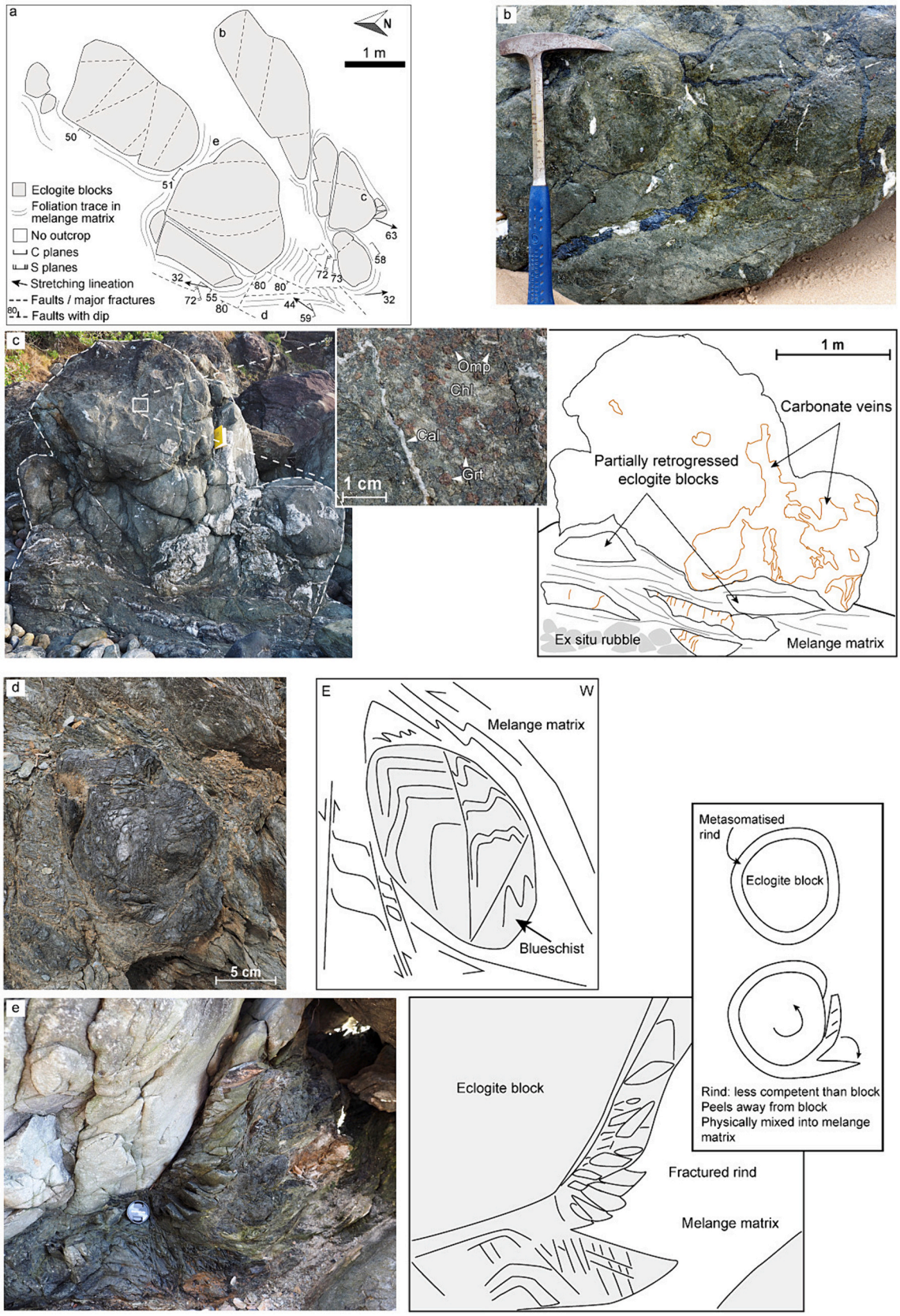


**Fig. 6.** Lithologies and structures in the central section. (a) Map of most of the eclogite blocks within the central section showing their jigsaw fit. The letters b-e note the position of features highlighted in figures b-e. (b) Veins of Gl + Ph cross-cutting an eclogite block. (c) An in situ eclogite block with left inset showing mineralogy and right inset showing the major features of the photograph. (d) A folded blueschist σ-type object in mélange matrix. (e) Edge of an eclogite block that shows a fractured rind that has peeled away from the block and preserved part way through the process of progressively physically mixing into the mélange matrix.

eclogite layer that show appear to have once been continuous, but are now separated by a vein of Grt-Ph schist (Fig. 5c,d). Phengite contains 3.42–3.68 Si p.f.u. and XMg of 0.6–0.77 (Table S1). Glaucophane occurs as euhedral to anhedral crystals in layers and in boudin necks that separate Omp-rich layers (Figs. 4c, 5e, S2a). Glaucophane is occasionally zoned with Mg-rich cores and Fe-rich rims with XMg varying between 0.38 and 0.46 (Table S1). Oriented glaucophane defines the foliation and contains parallel layers of titanite. Rutile occurs in veins that crosscut the foliation in omphacites and blueschists and is partially to completely replaced by titanite. Titanite is tens of microns in diameter, occurs in discontinuous layers, and appears in highest concentration in Grt-Ph schists (Fig. 4b, c) and blueschists. Titanite contains up to 2.69 wt% $Al_2O_3$ and up to 1.63 wt% FeO (Table S1). Pyrite is up to 1 mm length and euhedral to anhedral (Figs. 4c, S2a opaque mineral).

Overprinting relationships between the different layers indicate their relative timing (Figs. 4c, 5c,e). At contacts with Grt-Ph schists or blueschists, omphacitites are fractured and included in the Ph + Ttn or glaucophane matrix, indicating the Grt-Ph schist and blueschist layers formed after the omphacitites (yellow arrows in Figs. 4c, 5e, S2e). This relative timing is also demonstrated in layers where glaucophane has partially replaced omphacite at the boundary between the two layers. Glaucophane also appears in veins that crosscut Grt-Ph schists, eclogites and omphacitites, indicating these blueschist veins also formed after Grt-Ph schists (Figs. 5e, S1b). Layers of Lws-omphacitite occasionally grade into omphacitites, with no crosscutting relationships evident (Fig. S2f).

### 4.2. Central section

The central section is distinguished from the southern section by lack of layering and folding in former eclogite facies blocks.

#### 4.2.1. Central section lithologies

Blocks in the central section are round to elongate, up to 8 m in length, and contained in a mélange matrix that consists of talc, chlorite, tremolite and carbonate in regions close to mafic blocks and serpentine, titanite and carbonate close to peridotite blocks. The mafic blocks in this section consist of partially retrogressed eclogites and Ph-omphacitites. Eclogites are defined as rocks where omphacite and garnet show equilibrium textures and are referred to as former eclogites because they have been partially to completely retrogressed to Chl + Ph + Ttn ± Pmp. Retrogression is more pervasive on the edges of blocks adjacent to mélange matrix. Within the central section, former eclogites are confined to a 20 m-long section (Figs. 2, 6a) and are massive and unfoliated (Fig. 6b, c). The jigsaw fit of most of the individual blocks suggests they once formed a continous, lens-shaped block approximately 20 m long and 10 m wide (Fig. 6a). In outcrop former eclogite blocks appear as green (omphacite and/or chlorite) blocks with red garnets up to 5 mm diameter (Fig. 6c). Blocks are dissected by carbonate veins that show no preferred orientation within blocks, but parallel the foliation in the matrix outside blocks (Fig. 6c).

#### 4.2.2. Central section structures

Minerals in former eclogite blocks do not show any alignment that suggests a foliation, although the extensive retrogression may mask pre-existing structures. The edges of some former eclogite blocks show internal fractures that calve off a wedge-shaped outer layer of the block (Fig. 6e). These wedges are either adjacent to the block or partially to completely separated from the block by mélange matrix. In one case, multiple wedge layers are evident, which lie at increasing angles from the block margin, separated by mélange matrix (Fig. 6e). Inside the wedge-shaped layer there is a set of parallel fractures that are approximately perpendicular to the long edge of the layer, and the external foliation.

Rare blueschist blocks are isoclinally folded with blocks a few cm in diameter preserved as isolated fold hinges and larger blocks folded and sheared into σ-type objects that show shear sense consistent with the mélange matrix foliation (Fig. 6d).

#### 4.2.3. Central section microstructures and mineral chemistry

A peak eclogite-facies mineral assemblage is recognised as garnet porphyroblasts that contain omphacite and rutile inclusions (Figs. 7a, S2g). Porphyroblasts are in a matrix of phengite, chlorite and titanite, which is interpreted to have formed during retrogression indicated by partial replacement of garnet by chlorite (Figs. 7a, S2g). Garnet is highly fractured and has euhedral to anhedral shapes. In PPL, garnet is inclusion rich, with decreasing inclusion abundance towards the rims and also contains anomalous inclusion-free patches. In addition to omphacite and rutile, garnet also has primary inclusions of Ph, Chl, Ap, and Qz, and secondary inclusions of Ttn, which partially replaces Rt (Fig. S2g). Rutile inclusions are up to 2 mm long and garnet fractures are infilled by coexisting Kfs + Qz or chlorite. Synchrotron element mapping revealed element zoning with garnet cores rich in Mn and depleted in Fe and a gradual decrease in Mn and increase in Fe towards the rim. Garnet is also zoned in Y with a depleted inner core (in the zone where Mn is enriched), surrounded by a zone of Y enrichment that encapsulates the Mn rich core, surrounded by a depleted edge (Fig. 7a). Microprobe analyses indicate garnet is $Alm_{36\text{-}69}Spss_{0\text{-}30}Grs_{23\text{-}54}Py_{0\text{–}06}$ with higher Spss and lower Alm and Py values in cores (Table S1).

In the matrix surrounding garnet porphyroblasts, titanite pseudomorphs former rutile and also appears as euhedral to anhedral crystals up to 0.5 mm long in the matrix with inclusions of zircon (Fig. S2g). Titanite contains up to 2.26 wt% $Al_2O_3$ and up to 0.91 wt% FeO (Table S1). Apart from titanite (about 5 % of the matrix), the matrix also contains phengite (60 %), chlorite (30 %) as well as minor zircon and apatite. Two types of chlorite are evident in PPL and BSE: a brown

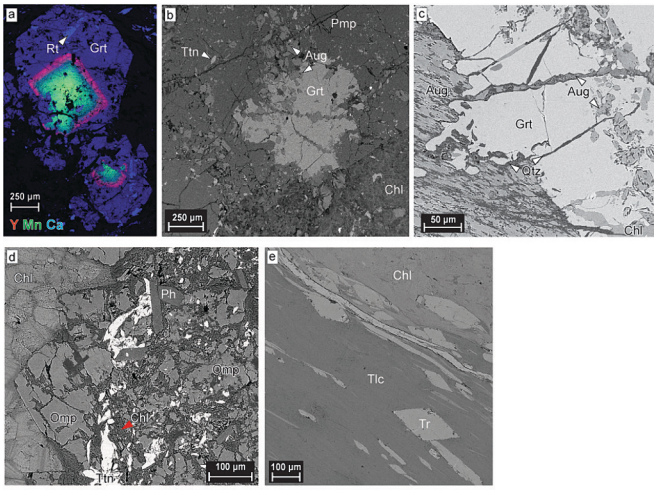


**Fig. 7.** Thin section images from rocks of the central section. (a) Synchrotron element maps of ytrium (red), manganese (green) and calcium (blue) showing garnet porphyroblasts with Mn and Y zoning. The lighter blue patches in garnet are rutile inclusions (see Fig. S2 for photomicrograph of this thin section). (b) Backscattered electron (BSE) image showing garnet porphyroblast with inclusions of augite, included within a pumpellyite porphyroblast. In the lower right corner, the matrix is evident, consisting of chlorite and titanite. (c) BSE image of the edge of a garnet porphyroblast with inclusions of augite. Garnet contains fractures filled with augite and/or quartz. Note that some augite-garnet interfaces contain discontinous rims of quartz. (d) BSE image of the edge of a chlorite vein (left hand side) in omphacitite. Omphacite is partially overprinted by an alteration assemblage of chlorite, phengite and titanite. Omphacite has euhedral crystal faces projecting into the chlorite vein, indicating that omphacite recrystallised during vein formation. (e) BSE image of the mélange matrix, which consists of talc, tremolite and chlorite in the central section. (For interpretation of the references to colour in this figure legend, the reader is referred to the web version of this article.)

anhedral, porous variety in the matrix that is high in Mg and low in Fe (Chl1; Fig. S2g), and a green, fibrous variety high in Fe and low in Mg (Chl2) that overprints the Chl1 + Ph matrix, does not show marked porosity in BSE and tends to occur in garnet fractures and adjacent to carbonate veins. Chl1 partially replaces garnet and occasionally pseudomorphs it (Fig. S2g). Chlorite has XMg between 0.39 and 0.68 and phengite contains 3.39–3.7 Si p.f.u. and XMg of 0.56–0.68 (Table S1).

At the western contact between eclogite blocks and mélange matrix, a different textural association of clinopyroxene and garnet is evident, which also shows different chemistry. Here, clinopyroxene is augite (Fig. 7c) with 21 wt% CaO, 11 wt% MgO and 4–5 wt% $Al_2O_3$, distinguishing it from the omphacitic clinopyroxene elsewhere in the central section. Garnet is also different here, forming anhedral porphyroblasts up to 5 mm in diameter, notably lacking rutile inclusions, although inclusions of chlorite, titanite, and augite are present (Fig. 7c). Here, garnet has similar zoning in Mn and Fe to that in other central section eclogites, except that cores are larger and less distinct, and Y zoning is confined to garnet cores rather than showing enrichment in a ring around Mn-rich cores (Fig. S2h). Garnet also contains fractures that are filled with augite with incomplete rims of quartz on the fracture walls (Fig. 7c). Garnet has a similar composition to garnet in other parts of the central section with $Alm_{36\text{-}66}Spss_{0\text{-}17}Grs_{24\text{-}54}Py_{0\text{–}03}$ (Table S1). Augite porphyroblasts are anhedral, up to 5 mm long and contain inclusions of quartz, carbonate and chlorite oriented parallel to the dominant augite cleavage plane, as well as unoriented garnet inclusions and veins. Many inclusions of garnet in augite are partially rimmed by quartz (Fig. 7c). Augite and garnet sit in a matrix of chlorite (70 %), pumpellyite (20 %) and titanite (5 %) with minor phengite. Chlorite forms anhedral patches that partially replace augite and has XMg between 0.45 and 0.73. Elongate prisms of pumpellyite up to 8 mm long are seen in this rock, and they include garnet, augite, and titanite (Fig. 7b).

In the central section, Ph-omphacitites have the same appearance in outcrop as the eclogites, with the notable absence of garnet. In thin section, they consist of omphacite (up to 200 μm), phengite (up to 200 μm), chlorite (very fine and anhedral), and veins of carbonate. Omphacite is anhedral and contains inclusions of titanite, quartz and zircon (Fig. 7d). It is partially retrogressed to fibrous brown chlorite in an alteration assemblage that also includes titanite and phengite (Fig. 7d). Phengite occurs as patches of unoriented laths up to 1 mm length. Omphacite, phengite, titanite and chlorite in Ph-omphacitites have the same composition as in other central section rocks (e.g., Mac3a analyses in Table S1).

One Ph-omphacitite block (Mac 3b) contains a vein of recrystallised, euhedral Omp + Chl + Cb + Ph (Fig. 7d) with titanite fringing part of the edge of the vein and appearing as layers and disseminations within the vein. Omphacite in the vein is up to 1 mm in length and forms light green to white euhedral crystals. Chlorite forms equidimensional flakes with sutured grain boundaries. Carbonate and titanite form anhedral crystals occasionally with small dihedral angles. On the edges of the vein, omphacite from the host rock shows euhedral crystal faces at contacts with carbonate or chlorite (Fig. 7d). This euhedral omphacite shows the same partial replacement by chlorite as the rest of the thin section, but vein omphacite is not retrogressed.

Blocks of blueschists in the central section form discontinuous layers up to 30 cm in length and consist of glaucophane and phengite with minor titanite (Fig. 6d). Blueschist veins composed of Gl ± Cb ± Py crosscut eclogites at the eastern side of the outcrop (Fig. 6a, b).

The mélange matrix to the mafic blocks in the central section consists of chlorite, tremolite and talc (Figs. 6, 7e). Chlorite in the matrix forms equidimensional to elongate crystals up to 200 μm long with cleavage parallel to the folded foliation (Fig. 7e). Chlorite contains 3–7 wt% $Cr_2O_3$ and XMg of 0.80 (Table S1). Tremolite forms euhedral prisms up to 0.5 mm long with long axes parallel to the foliation. Talc is anhedral and porous (Fig. 7e).

### 4.3. Northern section

The northern section is distinguished from the southern and central sections by the presence of intensely folded Lws-blueschists that show partial to complete retrogression to greenschists. The matrix here is similar to that in the central section, but with more carbonate, which increases in proportion close to a large carbonate block.

#### 4.3.1. Northern section lithologies

The northern section contains in situ blocks that are elongate to equant and up to 10 m in length, although in some places blueschist blocks are separated by narrow layers of matrix and show a jigsaw fit, indicating they once formed coherent blocks at least 20 m long (Fig. 2). Blueschists consist of Gl ± Lws + Ph + Ttn ± Omp ± Chl and many show a fine-grained matrix of Gl ± Ph that hosts mm-scale, discontinuous or boudinaged layers of Lws + Ph ± Ttn with rarer layers of coarse Gl + Lws (Fig. 8). Layers of Lws + Ph ± Ttn vary in the relative proportion of Lws and Ph, with some layers consisting of 90 % Lws, others 90 % Ph, and the rest with compositions between these end-members (Fig. 8). Titanite is present in most of these layers and in higher concentration in strain shadows of boudins (Fig. 8b).

#### 4.3.2. Northern section structures

In the northern section, small blocks of blueschist (< 30 cm) form isoclinal folds with axial planes approximately parallel to the foliation and fold axes parallel to the mineral stretching lineation defined by glaucophane in the block and chlorite in the matrix (Fig. 8a-c). Some folded blueschists have also been sheared into σ-type objects, as also seen in the central section (Fig. 6d). As highlighted in the previous section, Lws-blueschists contain layers with different relative proportions of Lws, Gl, and Ph. In thin section, it is evident that the layers are isoclinally folded and that fold limbs have been sheared apart from hinges, producing rootless fold hinges (Fig. 8a-c). Fold limbs are sheared into boudinaged layers, and some layers are completely sheared apart to form σ- or θ-type objects with Ph in pressure shadows (Fig. 8a-c) that show conflicting shear senses, suggesting pure or general shear. Surrounding competent folded layers is a matrix of very fine Gl that contains discontinuous patches of very fine Ph (Fig. 8a,b). The foliation and folded layering are overprinted by tension gashes filled with Ph + Cb (Fig. 8e).

Lws-blueschists that are partially retrogressed to greenschist typically form smaller blocks than unaffected Lws-blueschists. In thin section, thin, dark seams rich in titanite abruptly truncate the foliation, mineral grains, and veins of carbonate (Fig. 8f,g). In some cases, it is evident that there is 'missing material'; that is, part of a vein has been dissolved offsetting it on either side of the seam (Fig. 8e-g). Thus, these seams are interpreted to have formed during pressure solution. Interestingly, some rocks show evidence for several orientations of pressure solution seams, with early-formed seams parallel to the foliation truncated by later seams at high angle to the foliation (Fig. 8d, e, g). Some early-formed seams are also folded. We interpret this feature to be due to rotation of the block within the mélange matrix, causing a change in the orientation of maximum stress relative to the foliation and therefore the angle between foliation and pressure solution seams.

Lws-Chl schists (greenschists) show the same microstructure as Lws-blueschists, but contain more pressure solution seams, which have partially to completely dissolved Lws-Ph layers (Fig. 8g). Greenschists lacking lawsonite perhaps demonstrate the end result of this process, where only the pressure solution seam remains, with no preservation of the pre-existing compositional layering (Fig. 8f). In greenschists that show pressure solution, cuspate folds lined with titanite are evident (Fig. 8f).

#### 4.3.3. Northern section microstructures and mineralogy

Glaucophane is generally 5–10 μm long and forms euhedral – subhedral prisms with long axes mostly parallel to the foliation and layering

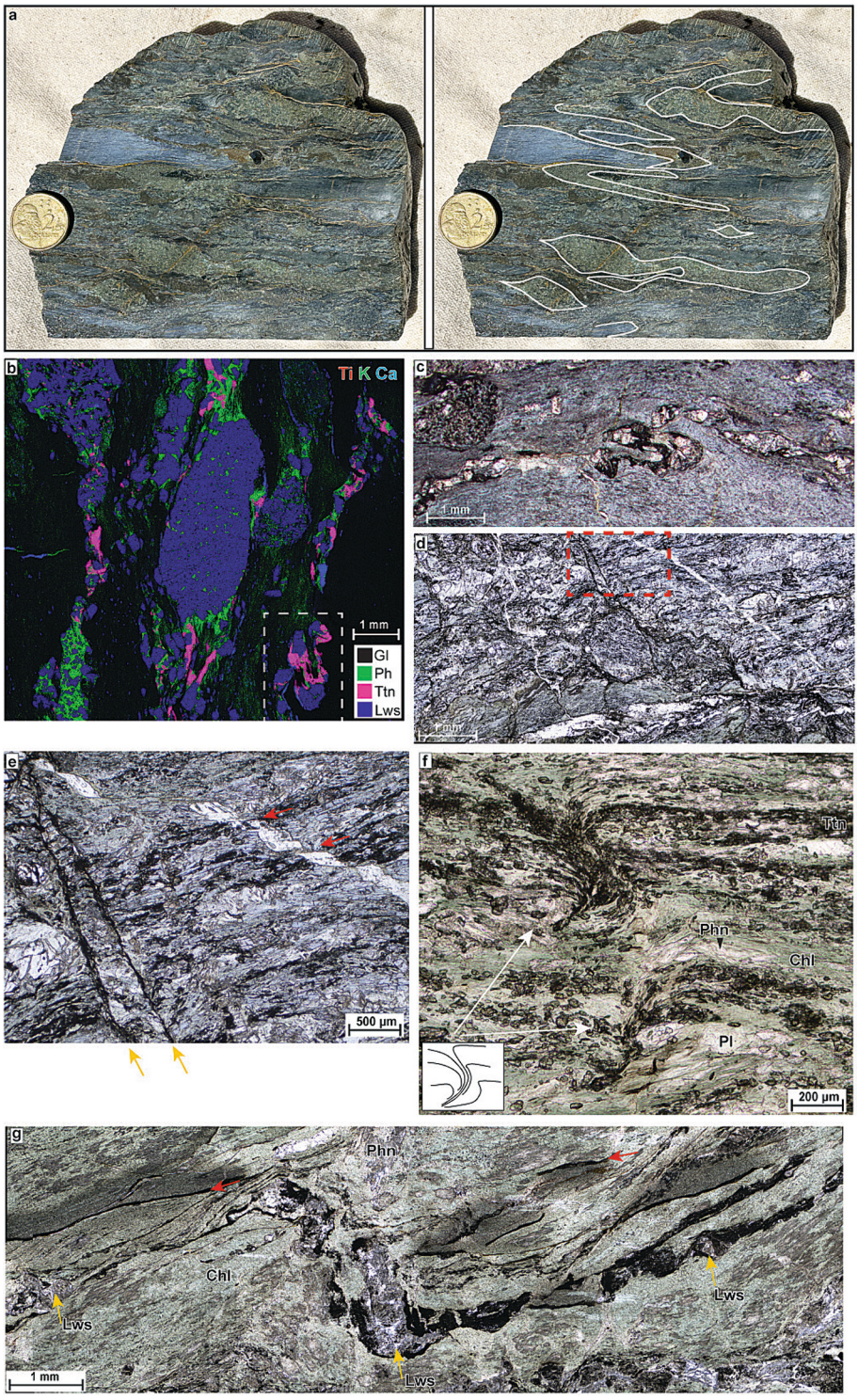


**Fig. 8.** Examples of lithologies from the northern section. (a) Lws-blueschist with folded centimetre-scale layering where boudinaged fold limbs form σ-type objects. (b) Synchotron element map of titanium (red), potassium (green) and calcium (blue) of a Lws-blueschist. Note the mm-scale folding and boudinage of layers. Area in dashed box is part of (c). (c) Photomicrograph of mm-scale fold in Lws-Ttn layer with boudinaged limbs (PPL). (d) Photomicrograph of blueschist with pressure solution seams (thin black layers). Red box denotes area shown in (e) (PPL). (e) Zoom in of (d) showing pressure solution seams parallel (red arrows) and perpendicular (yellow arrows) to the folation. Note the missing material in the calcite vein, dissolved by pressure solution. (f) Cuspate folds in greenschist (arrows; PPL). (g) Photomicrograph of pressure solution seams in greenschist (e.g., red arrows), marked by a high concentration of Ttn (black) and occasional crystals of Lws (yellow arrows). Note that where the main layer is perpendicular to the shortening direction (left of centre), Lws grains are preserved (PPL). (For interpretation of the references to colour in this figure legend, the reader is referred to the web version of this article.)

(Fig. 8c-e). Phengite occurs in isolated patches in the glaucophane-rich matrix and forms laths up to 100 μm long with long axes that define the foliation. Phengite contains 3.40–3.81 Si p.f.u. and has XMg of 0.61–0.78 (Table S1). Glaucophane also appears in rare layers of randomly oriented Ph + Gl ± Omp where it is up to 40 μm long. Both forms of glaucophane show patchy zoning in Fe and Mg in BSE images with XMg of 0.46–0.58 and minor incorporation of MnO (up to 0.62 wt %), CaO (up to 2 wt%) and $TiO_2$ (up to 0.69 wt%). Lawsonite forms euhedral porphyroblasts up to 200 μm in a matrix of Ph ± Ttn and contains inclusions of quartz, titanite and pyrite. It contains up to 1.95 wt% $TiO_2$ and up to 0.85 wt% FeO. Omphacite (up to 0.5 mm) forms rare blocky porphyroblasts that are pale green in PPL and partly retrogressed to chlorite. Microprobe analyses indicate that they have the same composition as omphacite in eclogites from the southern and central sections in major elements as well as the incorporation of small proportions of TiO2 (up to 0.12 wt%) and MnO (up to 0.48 wt%) (Table S1). Veins of quartz and carbonate are approximately perpendicular to the foliation and occasionally terminate abruptly in titanite-rich layers (Fig. 8d,e).

Some blueschists and Lws-blueschists show partial replacement of glaucophane by chlorite, and are interpreted as transitional to greenschist facies. These blocks contain less Lws than Lws-blueschists and Lws is partly retrogressed to pseudomorphs of fine, white mica (Fig. 8g), requiring the presence of a K-rich fluid (Hamelin et al., 2018). Lawsonite is concentrated in layers, as in the non-retrogressed blueschists, but these layers lens into dark, irregular, discontinuous pressure solution seams, described further in Section 4.3.2 (Fig. 8g). In some blocks, retrogression to greenschist facies is complete and the matrix of Chl + Ttn alternates with darker Ttn-rich layers (Fig. 8f, g).

#### 4.3.4. *Watonga formation contact with northern section*

The contacts between the Watonga Formation block and the blueschists of the RBMM are not exposed. North of the northern contact there is a 3-m wide lens of RBMM blueschist blocks in chlorite-tremolite matrix, south of the contact with the Port Macquarie serpentinite (Fig. 2). The contact between the RBMM and the Port Macquarie Serpentinite is presumed to be a brittle fault (Fig. 2), marked by a break in the outcrop with a change in the foliation strike on either side of the contact (Fig. 2). Outcrop of Port Macquarie Serpentinite adjacent to the presumed fault shows normal shearing on sharp shear planes overprinting ductile thrusting (Fig. 2). The sharp normal shear planes are approximately parallel to the orientation of the presumed fault, suggesting that the fault may have been of the same generation and had normal offset. Within a metre of the northern contact with the RBMM, the Port Macquarie Serpentinite contains rounded blocks of blueschist. Beyond (north of) this, the serpentinite encases lenses of peridotite exclusively.

### 4.4. *RBMM mélange matrix structures*

The mélange matrix has a variable orientation as it wraps around rigid blocks, but generally has a N*E*-SW trend, dipping moderately to the NW (Fig. 2 stereonet inset). The stretching lineation is defined by chlorite and glaucophane and generally plunges moderately to the NE or SW (Fig. 2 inset). In the central section, the matrix shows disharmonic, isoclinal folding with non-cylindrical fold axes and fold wavelengths up to 5 cm. Fold axes are highly variable, but show the same range of plunge orientations as the stretching lineation (Fig. 2 inset). Although in thin section the folds are complexly refolded (Fig. 9b), a larger scale orientation and asymmetry is evident in outcrop, indicating top-to-E thrust shearing. There are also rare σ-type objects in smaller blueschist blocks that also show top-to-E thrust shearing (Fig. 6d).

In the northern section, where there are fewer blocks and the matrix contains more carbonate, the matrix structures are similar to those in the other sections with the same NW trend, with foliation transposed into parallelism with the edges of competent blocks when in close proximity

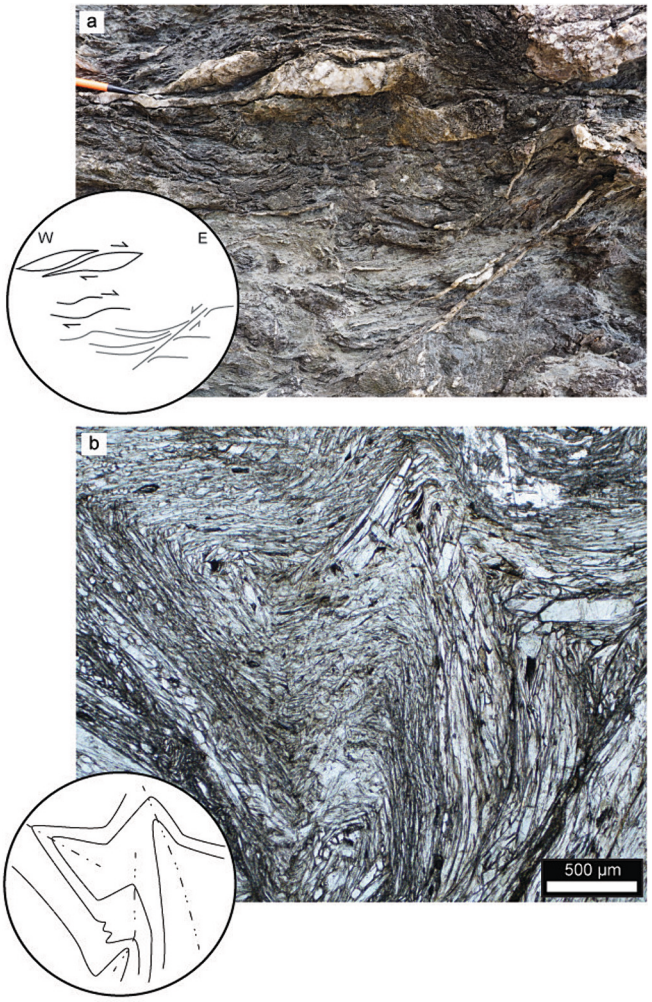


**Fig. 9.** Mélange matrix structures. (a) Thrust shearing overprinted by normal shearing in the serpentinite-dominated matrix. (b) Photomicrograph of folded Talc-Tre-Chl mélange matrix (PPL).

to them. However, there are two notable differences between the matrix structures in the northern and central sections: (1) isoclinal folds are ubiquitous in the central section, but absent from the northern section, and (2) in the northern section, there is evidence of thrust shearing (D1) overprinted by normal shearing (D2; Fig. 9a). The orientation of D1 and D2 structures means that this relationship can only be observed in rare E-W trending gullies eroded into the cliff face. In these regions, S1 C planes dip moderately W and, together with S planes that dip steeply N and a down dip stretching lineation, indicate top-to-E thrust shearing, consistent with observations in the central section. S1 C planes are locally sheared by moderately-steeply N-dipping shear planes that show a top-to-N, normal shear sense (Fig. 9a). Normal shear sense is also interpreted for brittle faults throughout the area (Fig. 2). These faults dip steeply in a range of orientations that vary from SW to NE dipping and they mostly crosscut blocks at high angles to their long axes.

## 5. Evidence for high pressure metasomatism

Mafic blocks in the RBMM are partially to completely retrogressed at least in two hydration stages in the blueschist and greenschist facies. We suggest that there is also evidence for metasomatism at eclogite facies in the rocks of the southern section. As described in section 4.1.1, these rocks contain alternating layers of eclogite, omphacitite and Grt-Ph schist and there are two possible origins for these layers: (1) layers of different composition reflect primary compositional differences in the

protolith or (2) layers of omphacitite and Grt-Ph schist formed due to metasomatic alteration of eclogite. We believe the latter option more likely because there is evidence for the presence of a fluid during the formation of layers of Grt-Ph schist and Lws-omphacitite. Textures that have been identified in the literature as unequivocally indicative of mass transfer during fluid-rock interaction include crack-seal veins, incomplete reaction rims at the interface between two minerals, porosity in metamorphic minerals, crystals that grew into the fluid with crystal faces against the former fluid phase, and irregular mineral zoning features such as oscillatory zoning, embayments and truncated zoning patterns (e.g., Ague and Axler, 2016; Goncalves et al., 2013; Putnis, 2009; Putnis and Austrheim, 2010; Rubatto et al., 2020). We see several of these textures in the Grt-Ph schist and omphacitite layers, which are summarised here and in Fig. 5. One key texture indicative of formation of Grt-Ph schist layers during metasomatism is the growth of phengite perpendicular to fractures in omphacitite layers (Fig. 5c, d), which indicates vein formation and evidence of the presence of a fluid during formation of Grt-Ph layers (Bons et al., 2012). Another key texture in Grt-Ph schist layers is the presence of porosity in the Ph-Ttn matrix (Fig. 5a), which indicates the presence of a fluid phase during mineral growth. Another key texture we see in southern section eclogite facies rocks is irregular zoning patterns in garnet in the Grt-Ph schist and in lawsonite in the Lws-omphacitites. As described in Section 4.1.3, garnet in Grt-Ph schist layers exhibits oscillatory zoning in Mn (and to a lesser extent, Y) as well as zoning in embayments and truncated zoning patterns (Fig. 5a). These features form when pre-existing garnet grains interact with a fluid that was not in chemical equilibrium with the garnet, causing dissolution of the rim of the garnet into the fluid and precipitation of a new garnet zone with a different composition (Rubatto et al., 2020). The higher concentration of Mn and Y is due to the incorporation of these elements into the fluid during garnet dissolution, and their precipitation in higher concentrations when the new zone forms. Truncated zoning and zoning in embayments is particularly convincing evidence of fluid-rock interaction. While mineral zones can form during prograde metamorphism in the absence of fluids, mineral zones will be complete, since the entire mineral is undergoing metamorphism at the same time (Putnis, 2009). Incomplete zoning occurs when a fluid interacts with just one part of the garnet crystal, with the new zone growing where the fluid-grain interaction has taken place (Putnis, 2009). Oscillatory, irregular Mn zoning in garnet in Ph-Grt schists has been found in eclogites in other subduction channels and has also been interpreted as indicative of dissolution-precipitation in those regions (e.g., Angiboust et al., 2014; Erambert and Austrheim, 1993; Giuntoli et al., 2018; Hyppolito et al., 2019; Lanari et al., 2017; Vho et al., 2020; Zack et al., 2002).

In the Grt-Ph schists matrix lawsonite, phengite, omphacite and chlorite are in apparent textural equilibrium with the metasomatic garnet, or at least their rims (Figs. 4c, S1). We also see that matrix Ttn is included in garnet cores and oscillatory zones and embayments and that the alignment of Ttn inside garnet porphyroblasts (internal foliation) is continuous with the Ttn-bearing foliation (external foliation) and the foliation wraps around the Grt porphyroblasts (4b,c), suggesting that the oscillatory zoned garnet grew at the same time as the Ttn + Ph. This suggests that the Ph-Ttn matrix (re)crystallised during the metasomatic event/s that formed the oscillatory zoning in garnet, suggesting local equilibrium between the minerals in the Ph-Ttn matrix and the oscillatory zoned garnet.

Mineral zoning is also seen in lawsonite in Lws-omphacitites as incomplete Sr zones and Sr zoning in embayments, similar to that observed in garnet in the Grt-Ph schists. We also note that garnet-free omphacitites are not the typical rock expected of MORB at eclogite facies (Chapman et al., 2019; Tian and Wei, 2014). Nevertheless, omphacitites are reported as eclogite facies rocks from subduction channels in Greece, Guatemala, Myanmar, Italy and Japan (e.g., Brocker and Enders, 1999; Giuntoli et al., 2024; Harlow et al., 2016; Nishiyama et al., 2017). They may be a result of a prograde decarbonation reaction that takes the general form of glaucophane + quartz + calcite = omphacite + $CO_2$ + $H_2O$ (Bröcker and Enders, 2001; Dixon and Ridley, 1987), or precipitation from a subduction fluid (Harlow et al., 2016), or may form from a pyroxenite by the metasomatic jadeitisation of pyroxene (Ng et al., 2016). These mechanisms all require involvement of a fluid at the high pressures of Lws + Omp stability.

Another distinctive texture in layered eclogite facies rocks of the southern section is the inclusion of brecciated pieces of adjacent eclogites and omphacitites into layers of Grt-Ph schist (Figs. 5e, S2e). The brecciated pieces have straight edges and a jigsaw fit with each other and with the adjacent layers that they were sourced from (Figs. 5e, S2e). One explanation for this texture might be that the Grt-Ph schist is a shear zone that entrained pieces of the competent omphacitite into it during shearing. However, in some regions within the Grt-Ph schist phengite does not show a preferred orientation and appears randomly oriented, suggesting the schist did not accumulate much strain and that this is not a viable explanation for this texture. An alternative explanation is that pieces of the omphacitite were fractured during the infiltration of high-pressure fluids during the metasomatism that formed the Grt-Ph schist layers.

Comparison of the omphacitite and Grt-Ph schist layers to standard MORB (Sun and McDonough, 1989) reveals that omphacitites contain more MgO and $TiO_2$ than MORB whereas Grt-Ph schist contains more $K_2O$, $TiO_2$ and $Al_2O_3$ (Table 3). Enrichment in MgO, TiO2, $Al_2O_3$ and $K_2O$ is also reported in metasomatized eclogites from other exhumed subduction channels (Angiboust et al., 2014; Sorensen et al., 1997) and can be related to high solubilities of these elements or, particularly in the case of $TiO_2$, high enthalpy of dissolution and a low barrier for nucleation (Audétat and Keppler, 2005).

As mentioned earlier, an alternative hypothesis for layers of different mineralogy in these rocks is that there were pre-existing compositional differences between the different layers prior to metamorphism that controlled the metamorphic assemblage that formed at high pressure. Such a model cannot explain (1) the appearance of 'ripped up' clasts of omphacitite in the Grt-Ph schist (Figs. 5e, S2e,f), (2) the fluid-mediated growth of garnet in Grt-Ph schists and lawsonite in Lws-omphacitites, as indicated by the mineral zoning textures (Fig. 5a,b), (3) elongate blocky fringes of phengite on fractures within omphacitite and eclogite layers (Fig. 5c,d), (4) layers of omphacitite, which have compositions inconsistent with any known protolith and are attributed to fluid-mediated processes in other subduction channels worldwide (e.g., Brocker and Enders, 1999; Giuntoli et al., 2024; Harlow et al., 2016; Nishiyama et al., 2017). As such, we interpret the layers of Grt-Ph schist and Lws-omphacitite to have formed during high pressure metasomatism in subduction channels.

To understand the PT conditions of this high pressure metasomatism we employed thermodynamic modelling, as described in the next section. New minerals that form during metasomatism have a composition that is in equilibrium with the composition of the fluid, the local equilibrium bulk rock, and the prevailing pressure and temperature conditions (e.g., Goncalves et al., 2013). The mobility of elements in the minerals and fluid controls the adjustment in bulk composition and the extent of change (Evans et al., 2013; Korzhinskii, 1959; Thompson, 1955). Therefore, minerals that grew during or were adjusted by metasomatism can provide information on the metamorphic grade at the time of fluid-rock interaction (e.g., Angiboust et al., 2014; Goncalves et al., 2013).

### 5.1. Phase equilibria modelling

#### 5.1.1. Pristine metabasalt

The PT conditions were assessed based on predictions of stable assemblages from phase equilibria modelling. Ideally an equilibrium assemblage from the central section would have been employed for pseudosection modelling to determine conditions of peak metamorphism, but this area was pervasively retrogressed. Accordingly, a

pristine blueschist sample from the northern section was used as the basis for pseudosection modelling and the determination of the conditions of metamorphism using mineral modes and compositional data.

Fig. 10 shows the results of pseudosection modelling for the selected mafic bulk rock composition. The preservation of lawsonite in the metabasalt restricts stability of prograde, peak and retrograde metamorphism to temperatures less than 540 °C and pressure greater than 10 kbar (e.g., Chapman and Clarke, 2021; Clarke et al., 2006). Late stage greenschist retrogression involved the destabilisation of lawsonite for chlorite–muscovite–actinolite assemblages. Peak conditions for the metabasalt can be inferred based on lawsonite coexisting with garnet, phengite, glaucophane, omphacite and rutile. Omphacite is variably preserved in the metabasaltic blocks, though is often armoured as inclusions in the mantle or rims of garnet porphyroblasts. This peak assemblage is best matched by the trivariant field at pressures of 22–28 kbar and temperatures of ~505–530 °C (Fig. 10a; Table 2). The relatively low Ca and Al, and high Mg of the selected bulk composition restricts lawsonite stability to higher temperatures and enables the persistence of high modes of glaucophane, consistent with that observed in blueschist blocks at Port Macquarie. The abundance of glaucophane and lower proportion of omphacite and garnet make the rock appear as a lawsonite blueschist that in fact is straddling eclogite facies *PT* conditions (cf. Wei and Clarke, 2011). A common MORB composition is predicted to have less glaucophane and more omphacite stable at these conditions (Chapman et al., 2019; Clarke et al., 2006; Tian and Wei, 2014; Wei and Clarke, 2011). Metastable predictions of biotite-absent equilibria additionally support the stabilisation of chlorite to higher-P that is more consistent with the observed mineral assemblages at Port Macquarie (Fig. S3). Isopleths of the jadeite component in omphacite (*j*(o)), excess silica in phengite ($XSi_{T1}$(mu)), and the grossular (*z*(g)) and almandine (*x*(g)) components of garnet overlap in the identified trivalent or quadravariant peak fields, but provide limited clear pressure estimates. Cases of glaucophane-rich rocks that contain garnet but lack lawsonite could be accounted for by metamorphism to slightly higher-*T*, consistent with the spread in isopleth uncertainties.

**Table 2**
The modal proportions of mineral phases for the field in Fig. 10 that correspond to the metamorphic events described in the text. P is in kbar and T in °C. Abbreviations are as defined for phase equilibria modelling in Section 3.2.

| PT | 25–505 | 25–515 | 25–515 | 24–515 | 17–425 | 17–450 |
|---|---|---|---|---|---|---|
| Event | Peak | Peak | Metasomatism | | Prograde | Retrograde |
| Minerals | bi-absent | bi-present | | | | |
| gl | 0.32 | 0.39 | | | 0.37 | 0.36 |
| o | 0.28 | 0.22 | 0.15 | 0.19 | 0.24 | 0.25 |
| g | 0.03 | 0.05 | 0.05 | 0.07 | | |
| mu | 0.13 | 0.08 | 0.48 | 0.46 | 0.13 | 0.14 |
| chl | 0.07 | | | 0.01 | 0.09 | 0.10 |
| ru | 0.01 | 0.01 | 0.01 | 0.01 | | |
| law | 0.01 | 0.06 | 0.16 | 0.10 | 0.02 | 0.00 |
| sph | | | | | 0.03 | 0.03 |
| bi | | 0.06 | 0.09 | 0.06 | 0.01 | |
| fluid | 0.13 | 0.14 | 0.07 | 0.09 | 0.12 | 0.13 |

Constraining aspects of the prograde metamorphic history is difficult, although the occurrence of phengite with titanite in some Lws-blueschist blocks that lack garnet suggests that the prograde *PT* path went through pressures of ~18 kbar and temperatures in the range of 400–450 °C. The preservation of lawsonite in many mafic lithologies requires the hairpin style *PT* path involving an initial retrograde event in blueschist facies at *P* of 15–18 kbar and *T* of 400–450 °C (e.g., Clarke et al., 2006). A subsequent greenschist overprint is consistent with final decompression at low-*T* (<400 °C). These conditions and the *PT* path are consistent with those suggested by Tamblyn et al. (2020b).

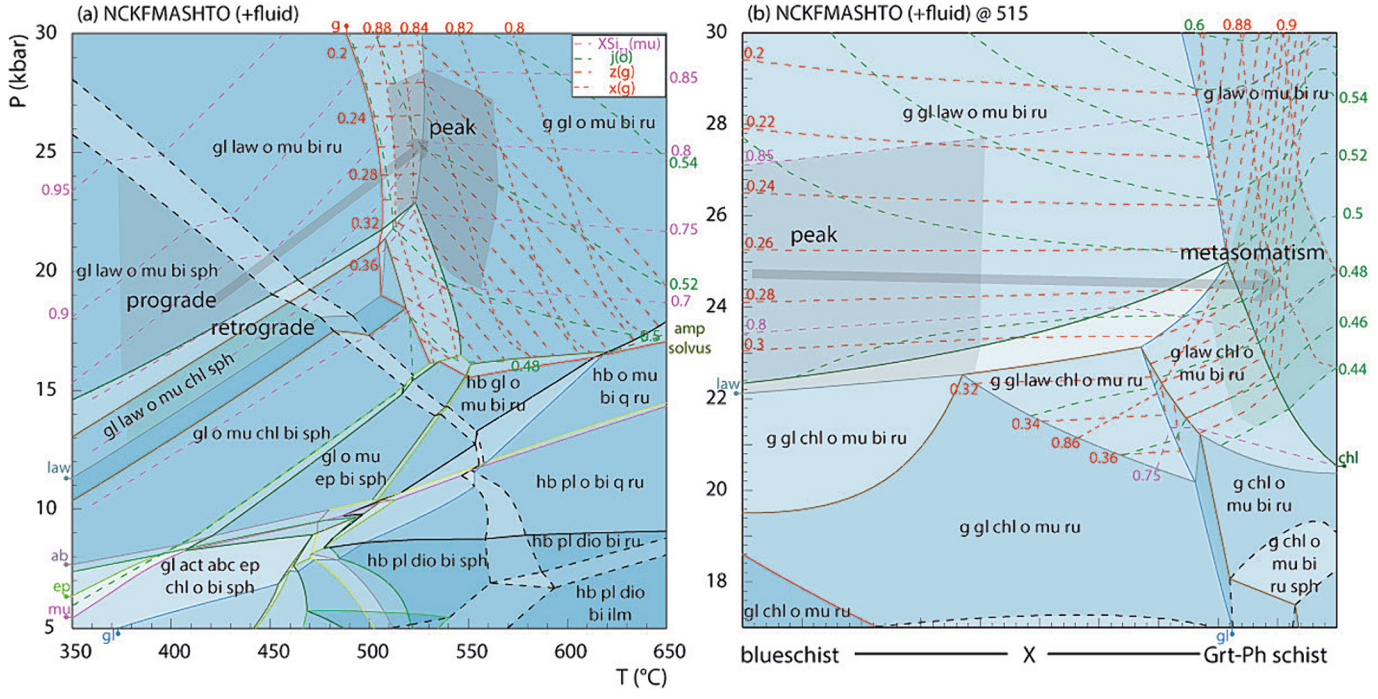


**Fig. 10.** Thermodynamic modelling of bulk compositions relevant to the RBMM. (a) *P–T* pseudosection for blueschist in the NCKFMASHTO system with fluid in excess. Different shading of the fields represents changes in variance of the phase assemblage. Mineral isopleths for garnet, omphacite and phengite are shown. Location of inferred prograde, peak, and retrograde metamorphic conditions are marked. (b) *P–X* pseudosection for the compositional change from blueschist (mole % = $H_2O$: 19.65; $SiO_2$: 44.26; $Al_2O_3$: 5.78; CaO: 4.68; MgO: 10.25; FeO: 8.08; $K_2O$: 0.92; $Na_2O$: 4.33; $TiO_2$: 0.98; O: 1.05) to Grt-Ph schist (mole % = $H_2O$: 19.66; $SiO_2$: 44.33; $Al_2O_3$: 10.58; CaO: 5.60; MgO: 6.16; FeO: 6.37; $K_2O$: 4.35; $Na_2O$: 0.75; $TiO_2$: 1.37; O: 0.84) in the NCKFMASHTO system with fluid in excess. Mineral isopleths for garnet, omphacite and phengite are shown. Location of inferred peak and metasomatism conditions are marked.

**Table 3**
Major element bulk rock composition normalised to oxidised average MORB composition of Sun and McDonough (1989) for key samples containing textures indicative of metasomatism at eclogite facies. Values <1 are depleted relative to MORB (e.g., mac3a contains 99 % $SiO_2$ of MORB) and > 1 are enriched (mac3a contains 469 % $K_2O$ of MORB).

| | Omphacitite (mac3a) | Lws-omphacitite (mac9a) | Omphacitite (mac1) | Grt-Ph schist (mac30a) |
|---|---|---|---|---|
| $SiO_2$ | 0.99 | 0.72 | 0.83 | 0.99 |
| $Al_2O_3$ | 0.79 | 1.01 | 0.93 | 1.39 |
| CaO | 0.87 | 0.66 | 0.23 | 0.97 |
| MgO | 1.43 | 2.55 | 2.36 | 0.39 |
| FeO | 0.71 | 1.42 | 1.54 | 0.90 |
| $K_2O$ | 4.69 | 0.03 | 0.09 | 23.99 |
| $Na_2O$ | 0.96 | 0.04 | 0.06 | 0.07 |
| $TiO_2$ | 2.33 | 0.62 | 1.87 | 4.55 |

#### 5.1.2. Garnet-phengite schist

Inherently, metasomatism presents complications to the simple application of equilibrium thermodynamics (Evans et al., 2013; White et al., 2004). Efficient buffering of rocks by an external fluid generally results in relatively high variance mineral assemblages with correspondingly small numbers of phases (e.g., Korzhinskii, 1959) that are not ideal for precise PT estimates (e.g., Powell and Holland, 2008). For this reason, modelling the near monomineralic omphacitite bulk compositions was avoided. Appropriate assignment of mobile components is additionally difficult due to challenges of predicting the exact composition of the fluid. Currently thermodynamic modelling has restricted capacity to resolve the complexities of fluid compositions beyond COHS-type (Evans et al., 2013). Additionally, the fluid volume required to produce the observed mineral assemblages is difficult to quantify. The fluid flux controls internal versus external buffering behaviour of the system, and thus the extent of mineralogical change (Elmer et al., 2006; White et al., 2004). Although, carbonate minerals are present in the blocks at Port Macquarie, they are mostly restricted to late veins that crosscut the Grt-Ph schist. Thus, a mixed $H_2O$–$CO_2$ fluid was not employed in this work. In the absence of reasonable constraints on fluid-rock ratios and fluid composition resolving the specific physicochemical changes during metasomatism of the Port Macquarie blueschist and eclogites is a challenge.

The *P-X* pseudosection at the inferred peak temperatures of 515 °C shows changes from the blueschist composition on the left-hand side to Grt-Ph schist on the right-hand side (Fig. 10b). The changes are mostly of low variance. The preservation of lawsonite during metasomatism provides a key lower limit on pressure conditions (>20 kbar). At pressures greater than 23 kbar the main change is the breakdown of glaucophane and the expansion of chlorite stability to slightly higher pressure and lawsonite to lower pressure. These changes are indicative of the large increase in muscovite and omphacite mode consistent with the observed assemblages in the Grt-Ph schist (Table 2). Garnet mode involves episodes of increase and decrease with changes in *X*, plausibly accounting for oscillatory zoning during resorption and precipitation phases. Mineral isopleths suggest that this mineral assemblage, formed during metasomatism, equilibrated at pressures similar to peak metamorphism (22–26 kbar) and are broadly consistent with phase equilibria modelled for the Grt-Ph schist by Tamblyn et al. (2020b). The crossover of phengite, omphacite and garnet isopleths occurs close to the upper pressure stability limit of chlorite and could account for its co-existence with high-pressure phases as a product of near-peak metasomatism rather than lower P-T retrogression. Titanite can be stable at these high-pressures if excess Ca and Ti are included in the bulk-rock and H is included within its crystal structure (e.g., Franz and Spear, 1985). Thus, addition of these elements via eclogite facies metasomatism can explain the high concentration of titanite in Ph + Grt layers and vein-like distribution in some samples. Although Ti is considered insoluble in $H_2O$ at typical crustal pressures, its solubility increases significantly in fluids at eclogite facies conditions (Mysen, 2019). Variability in the observed composition of the Grt-Ph schist was also modelled to investigate whether it caused any changes to the stability fields of key minerals or the conditions of metamorphism. A *P–X* pseudosection employing a Ph-Grt schist richer in titanium and calcium produces an expanded stability field of titanite and biotite (Fig. S3). The higher titanite mode also reduces the stability range of lawsonite and garnet. These variabilities could account for distinction in the modes of mineral assemblages in the different Grt-Ph rich layers. The absolute changes have minimal effect on the predicted conditions of metamorphism.

The high-pressure stability of titanite is confirmed in a *T–X* pseudosection calculated at fixed pressure of 27 kbar (Fig. 11a). A pronounced temperature-sensitivity is apparent for the main mineral assemblages in both the blueschist and Grt-Ph schist. This is particularly apparent for garnet and lawsonite but also rutile and titanite as compositions approach that of the Grt-Ph schist. A *P–X* pseudosection calculated at 450 °C (Fig. 11b) models assemblages during retrogression that are distinct from those preserved in the Grt-Ph schist. Garnet abundance is very low and consumed by chlorite and biotite at lower *P–T* conditions. The localised occurrence of chlorite and biotite in the Grt-Ph schist would be consistent with overprinting microstructures involving the partial pseudomorphs of garnet. Since omphacitite and eclogite layers are included in Ph + Grt schist layers (Figs. 4c, S2e), we infer that they formed at similar times or slightly earlier on the *PT* path, but still at eclogite facies conditions ($P > 20$ kbar and $T > 450$ °C).

## 6. Deformation of rocks generated during high pressure metasomatism

Sections 4 and 5 demonstrate that metasomatism at eclogite facies introduced layers of Grt-Ph schist and omphacitie into eclogites in the southern section. To understand how this process changed rheology we compare the structural evolution of these rocks to former eclogites from the central section that did not undergo eclogite facies metasomatism. In the section below we first discuss metamorphism and structures in central section rocks, before comparing them to rocks of the southern section.

As described in Section 4.2 an eclogite facies mineral assemblage is preserved in the central section, where omphacite inclusions are preserved in garnet porphyroblasts. The bell-shaped zoning profiles of Mn, Fe, and Y in garnet, with no evidence of oscillatory zoning or dissolution-precipitation processes suggests that they grew without significant modification by a fluid at eclogite facies. Blueschist facies retrogression in these rocks is limited to cross cutting veins of Gl ± Py and the edges of the blocks are extensively overprinted by a lower pressure assemblage of pumpellyite and chlorite. Thus, in addition to escaping metasomatism at eclogite facies, these blocks also avoided the moderate to extensive blueschist facies retrogression seen in the northern and southern sections. Accordingly, prior to extensive retrogression at the low pressures of pumpellyite and chorite stability, these blocks may have been eclogites sensu *strictu*, that is, blocks consisting predominantly of omphacite and garnet. We observe that these blocks exhibit rigid object behaviour within the strongly deformed matrix and show no evidence for intracrystalline deformation. As such, we interpret that these blocks are akin to the eclogites that behave as rigid blocks in other subduction channels, as described by Gao and Klemd (2003), Stöckhert (2002) and Stöckhert and Renner (1998).

In contrast, we find that the eclogite facies rocks of the southern section show a very different structural record and we suggest this is because of the lithological heterogeneity introduced to eclogites during metasomatism at eclogite facies. As described in Section 5, Grt-Ph schists formed within eclogites and omphacitites due to metasomatism at eclogite facies. The formation of weak phyllosilicate layers greatly reduced the strength of the rock and increased its anisotropy. Instead of behaving as rigid blocks like the eclogites in the central section, these layered eclogite facies rocks underwent isoclinal folding during

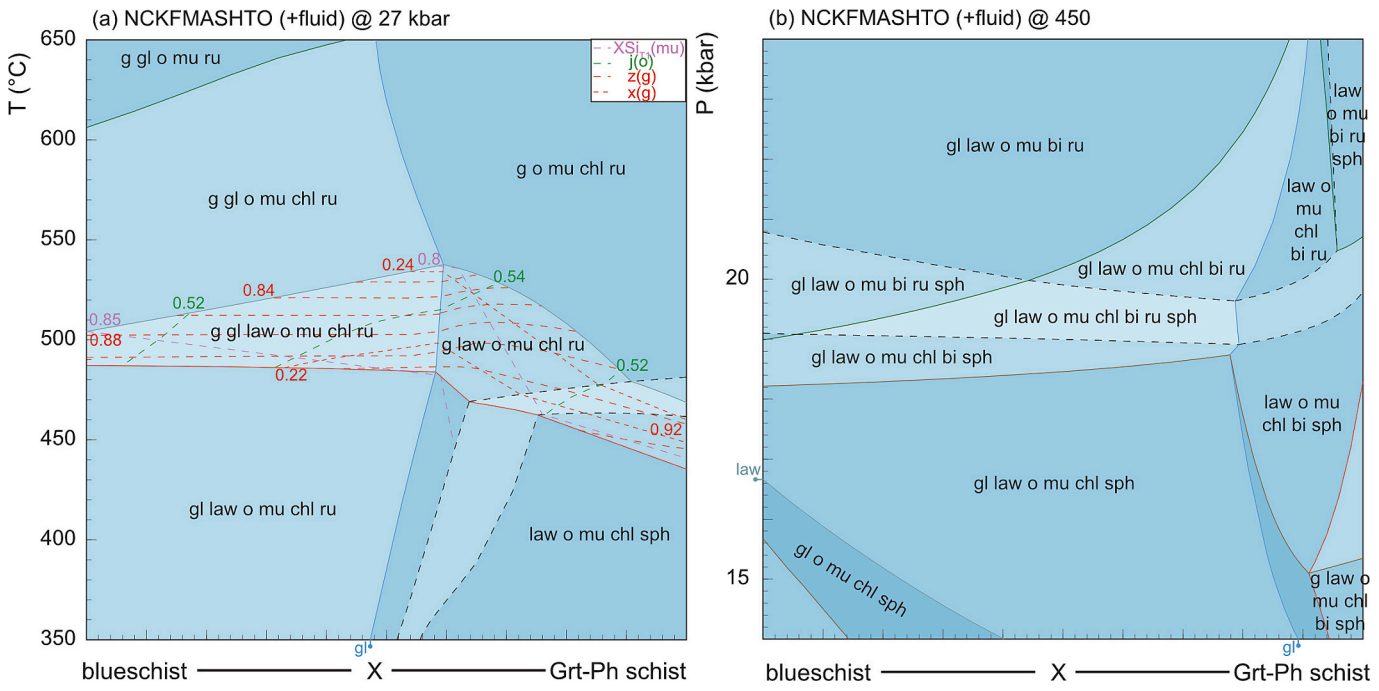


**Fig. 11.** Thermodynamic modelling to further constrain P-T for the compositional change from blueschist to Grt-Ph schist. (a) T-X pseudosection calculated at fixed pressure of 27 kbar for the compositional change from blueschist (mole % = H2O: 19.65; SiO2: 44.26; Al2O3: 5.78; CaO: 4.68; MgO: 10.25; FeO: 8.08; K2O: 0.92; Na2O: 4.33; TiO2: 0.98; O: 1.05) to Grt-Ph schist (mole % = H2O: 19.66; SiO2: 44.33; Al2O3: 10.58; CaO: 5.60; MgO: 6.16; FeO: 6.37; K2O: 4.35; Na2O: 0.75; TiO2: 1.37; O: 0.84) in the NCKFMASHTO system with fluid in excess. Mineral isopleths for garnet, omphacite and phengite are shown. (b) P-X pseudosection calculated at 450 °C for the same compositional change.

shearing. In Grt-Ph schist layers the partial alignment of phengite and titanite parallel to the folded layering in the rock (Fig. 4b,c) including within garnet porphyroblasts that grew during fluid-rock interaction, suggests that folding happened at the same time or after the metasomatism that produced these layers, which phase equilibria modelling indicates equilibrated at eclogite facies. In these eclogite facies rocks, veins of blueschist occur in fold limbs that have undergone boudinage (Fig. S2a) as well as in fold axial planes (Fig. S1b). Veins form along fold axial planes due to porosity created during shortening and this indicates that fluid ingress occurred during folding (Weinberg et al., 2015). Taken together, this indicates that folding began at eclogite facies and continued into blueschist facies, and therefore was occurring as the subduction channel was undergoing return flow. Folded blocks were further deformed in the returning part of the subduction channel with refolding of blocks as they rotated in the mélange matrix into type 2 fold interference patterns of Ramsay (1962) or into σ-type objects.

In the northern section, some blueschists show no evidence for higher-P metamorphism, so it is possible that they never reached pressure > 20 kbar and were simply incorporated into the subduction channel under return flow at shallower levels than the eclogite-facies blocks to the south. However, we found relict jadeite-rich omphacite in several Lws-blueschists and Ph-blueschists in the northern section, suggesting that at least some of the blueschists may record the obtainment of higher-P conditions. Lws-omphacitites that formed due to eclogite-facies metasomatism in the southern section may be the precursors to the Lws-blueschists that we see in the central section, since lawsonite in both rock types has identical major element compositions (Table S1) and shows the same hourglass Sr zoning. Although this is not necessarily conclusive evidence, we also see layered Lws-omphacitites and omphacite partially replaced by glaucophane, so it is reasonable to suggest a relationship between the two rock types. The major difference between Lws-omphacitites and Lws-blueschists is mm-scale layering and folding in the latter. This is due to the lower competence and higher anisotropy of glaucophane compared to omphacite, but this folding is only observed in blueschists that contain lawsonite layers, since it is competency contrast between lawsonite and glaucophane layers that produces the anisotropy required for folding during shearing. Segregation into glaucophane-rich and lawsonite-rich layers may be a result of pressure solution or shearing, both of which produce a differentiated fabric of this type (e.g., Finch et al., 2020; Platt et al., 2018). Pressure solution is the dominant deformation mechanism in many subduction channels (e.g., Behr and Platt, 2013; Stöckhert and Renner, 1998; Wassmann and Stöckhert, 2013), but it cannot produce both layering and folds without considerable reorientation of the block or the strain axes. We see examples where this has occurred in blocks, with pressure solution seams in multiple orientations and folded seams, but we do not see any evidence for those processes in samples of Lws-blueschist. Accordingly, we suggest that layering and subsequent folding were a result of shearing in the block during return flow. This suggests that at blueschist facies, shearing and mm-scale folding was the primary deformation mechanism affecting blocks in the RBMM. This process is readily evident on thin section scale but quite difficult to observe in outcrops, where rocks look like conglomerates (and have been previously referred to as such), comprising numerous pale rounded (clast-like) regions rich in lawsonite encapsulated in glaucophane-rich matrix. We find that these rounded regions are dismembered fold hinges, as can be observed on the hand sample and thin section scale.

The rocks of the northern section also demonstrate the structural evolution of blocks as they migrate from blueschist to greenschist conditions. At the transition from blueschist to greenschist facies, pressure solution becomes increasingly important, as evidenced by a gradual increase in the proportion of pressure solution seams (Fig. 8). One sample records partially formed pressure solution seams, where a layer of lawsonite has been partially consumed by the pressure solution seam (Fig. 8g). Some greenschist blocks preserve pressure solution seams parallel or sub-parallel to the foliation (Fig. 8g), but in others the seams are in multiple orientations (Fig. 8d), indicating changes in the direction of maximum stress over time. We interpret this to be a result of rotation of the block in the mélange matrix, producing pressure solution in different orientations and folding pre-existing seams and veins.

Dissolution-precipitation creep is also a possible mechanism, but we do not see any evidence for precipitation on a thin section to outcrop scale.

The RBMM records extensive deformation of blocks in the subduction channel during return flow from eclogite facies to greenschist facies. This is in contrast to many other subduction channels where blocks experienced minimal crystal-plastic deformation and behaved as rigid objects. The difference in the RBMM is extensive eclogite facies metasomatism, which introduced anisotropy and promoted strain localisation to the interior of some blocks, leaving less metasomatised blocks comparatively unaffected. Large-scale numerical models of subduction systems are commonly employed to understand how subduction systems operate and have provided an understanding of subduction channels and return flow that would have been impossible to elucidate otherwise (e.g., Gerya, 2022 and references therein; Gerya et al., 2002; Maierová et al., 2018). However, they rely on information from natural systems for model inputs. Our study indicates that while eclogites behave as competent blocks, other, weaker eclogite facies rocks can reduce the strength of the channel at these depths.

Competent eclogite blocks in the subduction channel increase its rheological heterogeneity and may cause stress amplification through block interaction (Beall et al., 2019b; Kotowski and Behr, 2019). Stress amplification is a result of "jamming" between rigid blocks, which is commonplace when they comprise >50 % of the subduction channel (Beall et al., 2019b). When block proportion reduces, aseismic slip is promoted. Our results indicate that in the RBMM eclogite facies metasomatism reduces subduction channel heterogeneity, as evidenced by the accumulation of ductile strain within these blocks. As such, this process also reduces the proportion of rigid blocks that may contribute to stress amplification and seismicity. This suggests that subduction channels that undergo widespread eclogite facies metasomatism may be less likely to generate seismic slip during return flow. However, the situation is likely to be more complex that this simple assertion implies, since the introduction of these weak layers adjacent to rigid omphacite-rich layers means that different layers will be achieving different strain rates, which will amplify stress between layers. This could potentially impact the type of slip within different layers in blocks, or the type of slip within the block overall.

## 7. Regional context of the RBMM

Tamblyn et al. (2020b) previously suggested that rocks of different ages and metamorphic grades were juxtaposed during return flow in the subduction channel shear zone at Port Macquarie. Eclogites from deep in the system were thought to have been juxtaposed with blueschists and greenschists as the shear zone incorporated new blocks at the same time as transporting blocks from deeper levels upwards. We suggest that some of the apparent juxtaposition of rocks of different metamorphic grade was caused by variation in the effectiveness of retrogression at different stages. The most competent blocks experienced less fluid infiltration and thus retained much of the peak metamorphic assemblage, whereas less competent domains were deformed and metasomatised, which enhanced deformation, creating a feedback effect that allowed their repeated retrogression as *PT* conditions decreased. Some blocks were likely eclogites that were comprehensively retrogressed to blueschist facies, and then partially retrogressed to greenschist facies. This process may have been a major contributor to the degradation of blocks into smaller sub-blocks, which then started to disperse (some clusters of the highest-grade blocks are today semi-contiguous), increasing the proportion of matrix.

The RBMM contains at least four distinct packages of rocks spanning metamorphic grades from sub-greenschist through to eclogite facies, including the Watonga Formation block and the southern, central, and northern sections. The mélange matrix that contains these blocks shows some compositional variation between sections, which might be interpreted to suggest that different sections of the subduction channel were juxtaposed by brittle faults seen in the region. However, the foliation in the mélange matrix and the deformation style is consistent between different sections, indicating that the northern, central and southern sections and the Watonga Formation block were part of the same system, juxtaposed at the later stages of return flow since the Watonga Formation is of low metamorphic grade. The RBMM was incorporated into the Port Macquarie serpentinite, which does not share the same orientation of foliation or shear sense, so did not undergo the same evolution as the RBMM matrix. Thus, the RBMM was deformed prior to incorporation into the Port Macquarie serpentinite.

Tamblyn et al. (2020b) interpreted that the RBMM underwent burial to eclogite facies (29 kbar), partial exhumation to at least 20 kbar, and then reburial to eclogite facies at ~450 Ma. Fukui et al. (1995) dated phengite from a blueschist in the RBMM and found an age of 467 ± 10 Ma, but it is not known whether this blueschist formed during prograde metamorphism, or during retrograde metamorphism during return flow. Phillips and Offler (2011) suggested that the high-pressure rocks in the nearby Peel-Manning Fault system were exhumed to blueschist facies during the Ordovician and then resided in the crust until the Permian, when they were incorporated into the Peel-Manning fault and brought to the surface. The RBMM shows a different evolution, of return flow to greenschist facies and juxtaposition against a block of Watonga Formation accretionary prism. Within the RBMM, greenschist facies metamorphism and the block of Watonga Formation have not been dated, but we assume that return flow to greenschist facies and juxtaposition with the Watonga Formation was a continuation of the return flow that started with the blueschist facies retrogression recorded in the eclogite-blueschist facies blocks within the Peel-Manning Fault System.

The northern and central sections show different structures in the mélange matrix, with *E*-vergent isoclinal folds ubiquitous throughout the central section and absent in the northern section, where S—C fabric is dominant. The shear sense in both locations is top-to-E thrust shearing, suggesting that the two regions show different structural expressions of the same deformation event. This may be because the two sections differ in both matrix mineralogy and block concentration, either of which could cause differences in their structural development. In the northern section, top-to-E thrust shearing was overprinted by sharp normal shear planes and faults. Although it is possible that present day orientations of structures have been rendered meaningless by rotation during exhumation, top-to-E thrust shearing is consistent with return flow on a W-dipping subduction zone, which is generally agreed to be the orientation of the subduction system when the RBMM eclogites formed, although there remains some controversy about some aspects of the system (Phillips and Offler, 2011). Incorporation of the RBMM into the Port Macquarie serpentinite and final exhumation was complete by the Permian, since eroded fragments of serpentinite are found in nearby early Permian rocks (Aitchison et al., 1994; Tamblyn et al., 2020b).

## 8. Conclusion

Eclogites in some subduction channels have been shown to accumulate little strain during shearing, behaving as rigid objects in the mélange matrix. We find that in the Rocky Beach Metamorphic Mélange, eclogite facies metasomatism significantly reduced the strength of blocks through the introduction of anisotropy and weak, phengite-rich layers. This modified the strength of the subduction channel, causing strain localisation to blocks that were folded and then refolded as they rotated in the mélange matrix during return flow. The RBMM also reveals how retrograde metamorphism including metasomatism changes the deformation mechanisms of rocks, promoting mm-scale folding at blueschist facies and then an increasing role for pressure solution as the metamorphic grade decreases. Competent eclogite blocks in the subduction channel increase its rheological heterogeneity and stress amplification due to block interactions can cause seismic slip events. Our results demonstrate that blocks that experience high pressure metasomatism prior to incorporation into the return flow section of the subduction channel can be less competent than rigid, unmetasomatised

eclogites. As such, subduction channels that experience widespread eclogite facies metasomatism may be less likely to generate seismic slip during return flow.

## CRediT authorship contribution statement

**M.A. Finch:** Writing – review & editing, Writing – original draft, Visualization, Validation, Supervision, Resources, Project administration, Methodology, Investigation, Funding acquisition, Formal analysis, Data curation, Conceptualization. **A. Olesch-Byrne:** Writing – review & editing, Methodology, Investigation, Formal analysis, Data curation, Conceptualization. **T. Chapman:** Writing – review & editing, Methodology, Formal analysis. **M. Beilharz:** Investigation, Formal analysis. **A. G. Tomkins:** Writing – review & editing, Resources, Methodology, Investigation, Funding acquisition, Conceptualization.

## Declaration of competing interest

The authors declare that they have no known competing financial interests or personal relationships that could have appeared to influence the work reported in this paper.

## Acknowledgements

We would like to thank editor Nadia Malaspina and reviewers Alissa Kotowski and an anonymous reviewer for feedback on this manuscript that improved the quality of the paper. This work was funded by an ARC Future Fellowship (FT180100533) to AGT and a Monash University Faculty of Science Advancing Women's Success grant to MAF. The authors acknowledge the use of instruments and scientific and technical assistance of Renji Pan and Xi-Ya Feng at the Monash Centre for Electron Microscopy, a node of Microscopy Australia. Part of this research was undertaken on the XFM beamline at the Australian Synchrotron (part of ANSTO), supported by beamtime grant AS212/XFM/17182 to all authors, and the authors gratefully acknowledge the scientific and technical assistance of beamline scientist, David Paterson.

## Appendix A. Supplementary data

Supplementary data to this article can be found online at https://doi.org/10.1016/j.lithos.2024.107797.

## References

Agard, P., Plunder, A., Angiboust, S., Bonnet, G., Ruh, J., 2018. The subduction plate interface: rock record and mechanical coupling (from long to short timescales). Lithos 320-321, 537–566.
Ague, J.J., Axler, J.A., 2016. Interface coupled dissolution-reprecipitation in garnet from subducted granulites and ultrahigh-pressure rocks revealed by phosphorous, sodium, and titanium zonation. Am. Mineral. 101, 1696–1699.
Aitchison, J.C., Blake Jr., M.C., Flood, P.G., Jayko, A.S., 1994. Paleozoic ophiolitic assemblages within the southern New England orogen of eastern Australia: implications for growth of the Gondwana margin. Tectonics 13, 1135–1149.
Allan, A.D., Leitch, E.C., 1992. The nature and origin of eclogite blocks in serpentinite from the Tamworth Belt, New England Fold Belt, eastern Australia. Aust. J. Earth Sci. 39, 29–35.
Angiboust, S., Pettke, T., De Hoog, J.C.M., Caron, B., Oncken, O., 2014. Channelized fluid flow and eclogite-facies metasomatism along the subduction shear zone. J. Petrol. 55, 883–916.
Audétat, A., Keppler, H., 2005. Solubility of rutile in subduction zone fluids, as determined by experiments in the hydrothermal diamond anvil cell. Earth Planet. Sci. Lett. 232, 393–402.
Barron, B., Scheibner, E., Slanskīĭ, E.N., 1976. A Dismembered Ophiolite Suite at Port Macquarie, New South Wales., Records of the Geological Survey of New South Wales 1889–1990. New South Wales Department of Mines, Sydney, Australia.
Beall, A., Fagereng, Å., Ellis, S., 2019a. Fracture and weakening of Jammed subduction shear zones, leading to the generation of slow slip events. Geochem. Geophys. Geosyst. 20, 4869–4884.
Beall, A., Fagereng, Å., Ellis, S., 2019b. Strength of strained two-phase mixtures: application to rapid creep and stress amplification in subduction zone mélange. Geophys. Res. Lett. 46, 169–178.
Behr, W.M., Platt, J.P., 2013. Rheological evolution of a Mediterranean subduction complex. J. Struct. Geol. 54, 136–155.
Bons, P.D., Elburg, M.A., Gomez-Rivas, E., 2012. A review of the formation of tectonic veins and their microstructures. J. Struct. Geol. 43, 33–62.
Brocker, M., Enders, M., 1999. U–Pb zircon geochronology of unusual eclogite-facies rocks from Syros and Tinos (Cyclades, Greece). Geol. Mag. 136, 111–118.
Bröcker, M., Enders, M., 2001. Unusual bulk-rock compositions in eclogite-facies rocks from Syros and Tinos (Cyclades, Greece): implications for U–Pb zircon geochronology. Chem. Geol. 175, 581–603.
Buckman, S., Nutman, A.P., Aitchison, J.C., Parker, J., Bembrick, S., Line, T., Hidaka, H., Kamiichi, T., 2015. The Watonga Formation and tacking point Gabbro, Port Macquarie, Australia: insights into crustal growth mechanisms on the eastern margin of Gondwana. Gondwana Res. 28, 133–151.
Chapman, T., Clarke, G.L., 2021. Cryptic evidence for the former presence of lawsonite in blueschist and eclogite. J. Metamorph. Geol. 39, 343–362.
Chapman, T., Clarke, G.L., Daczko, N.R., 2019. The role of buoyancy in the fate of ultra-high-pressure eclogite. Sci. Rep. 9, 19925.
Clarke, G.L., Powell, R., Fitzherbert, J.A., 2006. The lawsonite paradox: a comparison of field evidence and mineral equilibria modelling. J. Metamorph. Geol. 24, 715–725.
Cloos, M., 1982. Flow melanges: numerical modeling and geologic constraints on their origin in the Franciscan subduction complex, California. GSA Bull. 93, 330–345.
Cloos, M., Shreve, R.L., 1988a. Subduction-channel model of prism accretion, melange formation, sediment subduction, and subduction erosion at convergent plate margins: 1. Background and description. Pure Appl. Geophys. 128, 455–500.
Cloos, M., Shreve, R.L., 1988b. Subduction-channel model of prism accretion, melange formation, sediment subduction, and subduction erosion at convergent plate margins: 2. Implications and discussion. Pure Appl. Geophys. 128, 501–545.
Dixon, J.E., Ridley, J.R., 1987. Syros. In: Helgeson, H.C. (Ed.), Chemical Transport in Metasomatic Processes. Reidel, Dordrecht.
Elmer, F.L., White, R.W., Powell, R., 2006. Devolatilization of metabasic rocks during greenschist–amphibolite facies metamorphism. J. Metamorph. Geol. 24, 497–513.
Erambert, M., Austrheim, H., 1993. The effect of fluid and deformation on zoning and inclusion patterns in poly-metamorphic garnets. Contrib. Mineral. Petrol. 115, 204–214.
Evans, K.A., Powell, R., Frost, B.R., 2013. Using equilibrium thermodynamics in the study of metasomatic alteration, illustrated by an application to serpentinites. Lithos 168-169, 67–84.
Fagereng, Å., Sibson, R.H., 2010. Mélange rheology and seismic style. Geology 38, 751–754.
Festa, A., Pini, G.A., Dilek, Y., Codegone, G., 2010. Mélanges and mélange-forming processes: a historical overview and new concepts. Int. Geol. Rev. 52, 1040–1105.
Finch, M.A., Bons, P.D., Steinbach, F., Griera, A., Llorens, M.G., Gomez-Rivas, E., Ran, H., de Riese, T., 2020. The ephemeral development of C′ shear bands: a numerical modelling approach. J. Struct. Geol. 139, 104091.
Franz, G., Spear, F.S., 1985. Aluminous titanite (sphene) from the Eclogite Zone, south-central Tauern Window, Austria. Chem. Geol. 50, 33–46.
Fukui, S., Watanabe, T., Itaya, T., Leitch, E.C., 1995. Middle Ordovician high PT metamorphic rocks in eastern Australia: evidence from K-Ar ages. Tectonics 14, 1014–1020.
Gao, J., Klemd, R., 2003. Formation of HP–LT rocks and their tectonic implications in the western Tianshan Orogen, NW China: geochemical and age constraints. Lithos 66, 1–22.
Gerya, T., 2022. Numerical modeling of subduction: state of the art and future directions. Geosphere 18, 503–561.
Gerya, T.V., Stöckhert, B., Perchuk, A.L., 2002. Exhumation of high-pressure metamorphic rocks in a subduction channel: a numerical simulation. Tectonics 21, 1–6.
Giuntoli, F., Lanari, P., Engi, M., 2018. Deeply subducted continental fragments – part 1: fracturing, dissolution–precipitation, and diffusion processes recorded by garnet textures of the central Sesia Zone (western Italian Alps). Solid Earth 9, 167–189.
Giuntoli, F., Menegon, L., Siron, G., Cognigni, F., Leroux, H., Compagnoni, R., Rossi, M., Vitale Brovarone, A., 2024. Methane-hydrogen-rich fluid migration may trigger seismic failure in subduction zones at forearc depths. Nat. Commun. 15, 480.
Glen, R.A., 2005. The Tasmanides of eastern Australia. Geol. Soc. Lond. Spec. Publ. 246, 23–96.
Goncalves, P., Marquer, D., Oliot, E., Durand, C., 2013. Thermodynamic modeling and thermobarometry of metasomatised rocks. In: Harlov, D.E., Austrheim, H. (Eds.), Metasomatism and the Chemical Transformation of Rock. Springer-Verlag, Berlin Heidelberg, p. 53.
Green, E.C.R., White, R.W., Diener, J.F.A., Powell, R., Holland, T.J.B., Palin, R.M., 2016. Activity–composition relations for the calculation of partial melting equilibria in metabasic rocks. J. Metamorph. Geol. 34, 845–869.
Grigull, S., Krohe, A., Moos, C., Wassmann, S., Stöckhert, B., 2012. "Order from chaos": a field-based estimate on bulk rheology of tectonic mélanges formed in subduction zones. Tectonophysics 568-569, 86–101.
Gyomlai, T., Agard, P., Marschall, H.R., Jolivet, L., Gerdes, A., 2021. Metasomatism and deformation of block-in-matrix structures in Syros: the role of inheritance and fluid-rock interactions along the subduction interface. Lithos 386-387, 105996.
Hamelin, C., Brady, J.B., Cheney, J.T., Schumacher, J.C., Able, L.M., Sperry, A.J., 2018. Pseudomorphs after lawsonite from Syros, Greece. J. Petrol. 59, 2353–2384.
Harlow, G.E., Flores, K.E., Marschall, H.R., 2016. Fluid-mediated mass transfer from a paleosubduction channel to its mantle wedge: evidence from jadeitite and related rocks from the Guatemala Suture Zone. Lithos 258-259, 15–36.
Holland, T.J.B., Green, E.C.R., Powell, R., 2022. A thermodynamic model for feldspars in $KAlSi_3O_8$–$NaAlSi_3O_8$–$CaAl_2Si_2O_8$ for mineral equilibrium calculations. Journal of Metamorphic Geology 40 (4), 587–600.

Holland, T.J.B., Powell, R., 2011. An improved and extended internally consistent thermodynamic dataset for phases of petrological interest, involving a new equation of state for solids. Journal of Metamorphic Geology 29, 333–383.
Hyppolito, T., Cambeses, A., Angiboust, S., Raimondo, T., García-Casco, A., Juliani, C., 2019. Rehydration of eclogites and garnet-replacement processes during exhumation in the amphibolite facies. Geol. Soc. Lond. Spec. Publ. 478, 217–239.
Jessop, K., Daczko, N.R., Piazolo, S., 2019. Tectonic cycles of the New England Orogen, eastern Australia: a review. Aust. J. Earth Sci. 66, 459–496.
Kelley, K.A., Cottrell, E., 2009. ,Water and the Oxidation State of Subduction Zone. Magmas.Science 325, 605–607.
Kemp, A.I.S., Hawkesworth, C.J., Collins, W.J., Gray, C.M., Blevin, P.L., 2009. Isotopic evidence for rapid continental growth in an extensional accretionary orogen: the Tasmanides, eastern Australia. Earth Planet. Sci. Lett. 284, 455–466.
Korzhinskii, D.S., 1959. Physicochemical Basis of the Analysis of the Paragenesis of Minerals. Consultants Bureau Inc., New York.
Kotowski, A.J., Behr, W.M., 2019. Length scales and types of heterogeneities along the deep subduction interface: insights from exhumed rocks on Syros Island, Greece. Geosphere 15, 1038–1065.
Krebs, M., Maresch, W.V., Schertl, H.P., Münker, C., Baumann, A., Draper, G., Idleman, B., Trapp, E., 2008. The dynamics of intra-oceanic subduction zones: a direct comparison between fossil petrological evidence (Rio San Juan complex, Dominican Republic) and numerical simulation. Lithos 103, 106–137.
Lanari, P., Giuntoli, F., Loury, C., Burn, M., Engi, M., 2017. An inverse modeling approach to obtain P–T conditions of metamorphic stages involving garnet growth and resorption. Eur. J. Mineral. 29, 181–199.
Leitch, E.C., 1974. The geological development of the southern part of the New England Fold Belt. J. Geol. Soc. Aust. 21, 133–156.
Maierová, P., Schulmann, K., Gerya, T., 2018. Relamination styles in collisional orogens. Tectonics 37, 224–250.
Manton, R.J., Buckman, S., Nutman, A.P., Bennett, V.C., Belousova, E.A., 2017. U-Pb-Hf-REE-Ti zircon and REE garnet geochemistry of the Cambrian Attunga eclogite, New England orogen, Australia: implications for continental growth along eastern Gondwana. Tectonics 36, 1580–1613.
Marschall, H.R., Schumacher, J.C., 2012. Arc magmas sourced from melange diapirs in subduction zones. Nat. Geosci. 5, 862–867.
McNamara, D.D., Wheeler, J., Pearce, M., Prior, D.J., 2024. A key role for diffusion creep in eclogites: omphacite deformation in the Zermatt-Saas unit, Italian Alps. J. Struct. Geol. 179, 105033.
Mysen, B., 2019. Aqueous fluids as transport medium at high pressure and temperature: Ti4+ solubility, solution mechanisms, and fluid composition. Chem. Geol. 505, 57–65.
Ng, Y.-N., Shi, G.-H., Santosh, M., 2016. Titanite-bearing omphacitite from the Jade Tract, Myanmar: interpretation from mineral and trace element compositions. J. Asian Earth Sci. 117, 1–12.
Nishiyama, T., Mori, Y., Shigeno, M., 2017. Jadeitites and associated metasomatic rocks from serpentinite mélanges in the Nishisonogi unit, Nagasaki Metamorphic complex, western Kyushu, Japan: a review. J. Mineral. Petrol. Sci. 112, 197–216.
Och, D.J., Leitch, E.C., Caprarelli, G., Watanabe, T., 2003. Blueschist and eclogite in tectonic melange, Port Macquarie, New South Wales, Australia. Mineral. Mag. 67, 609–624.
Och, D.J., Leitch, E.C., Caprarelli, G., 2007. Geological Units of the Port Macquarie-Tacking Point Tract, North-Eastern Port Macqaurie Block, Mid North Coast Region of New South Wales. Quarterly Notes Geological Survey of New South Wales.
Peacock, S.M., Hyndman, R.D., 1999. Hydrous minerals in the mantle wedge and the maximum depth of subduction thrust earthquakes. Geophys. Res. Lett. 26, 2517–2520.
Penniston-Dorland, S.C., Harvey, K.M., 2023. Constraints on tectonic processes in subduction mélange: a review of insights from the Catalina Schist (CA, USA). Geosyst. Geoenviron. 2, 100190.
Penniston-Dorland, S.C., Kohn, M.J., Piccoli, P.M., 2018. A mélange of subduction temperatures: evidence from Zr-in-rutile thermometry for strengthening of the subduction interface. Earth Planet. Sci. Lett. 482, 525–535.
Phillips, G., Offler, R., 2011. Contrasting modes of eclogite and blueschist exhumation in a retreating subduction system: the Tasmanides, Australia. Gondwana Res. 19, 800–811.
Phillips, G., Offler, R., Rubatto, D., Phillips, D., 2015. High-pressure metamorphism in the southern New England orogen: implications for long-lived accretionary orogenesis in eastern Australia. Tectonics 34, 1979–2010.
Platt, J.P., Xia, H., Schmidt, W.L., 2018. Rheology and stress in subduction zones around the aseismic/seismic transition. Prog. Earth Planet. Sci. 5, 24.
Powell, R., Holland, T.J.B., 1988. An internally consistent dataset with uncertainties and correlations: 3. Applications to geobarometry, worked examples and a computer program. Journal of Metamorphic Geology 6, 173–204.
Powell, R., Holland, J.B., 2008. On thermobarometry. J. Metamorph. Geol. 26, 155–179.
Putnis, A., 2009. Mineral replacement reactions. Rev. Mineral. Geochem. 70, 87–124.
Putnis, A., Austrheim, H., 2010. Fluid-induced processes: metasomatism and metamorphism. Geofluids 10, 254–269.
Ramsay, J.G., 1962. Interference patterns produced by the superposition of folds of similar types. J. Geol. 70, 466–481.
Rubatto, D., Burger, M., Lanari, P., Hattendorf, B., Schwarz, G., Neff, C., Keresztes Schmidt, P., Hermann, J., Vho, A., Günther, D., 2020. Identification of growth mechanisms in metamorphic garnet by high-resolution trace element mapping with LA-ICP-TOFMS. Contrib. Mineral. Petrol. 175, 61.
Ryan, C.G., Siddons, D.P., Kirkham, R., Dunn, P.A., Kuczewski, A., Moorhead, G., De Geronimo, G., Paterson, D.J., de Jonge, M.D., Hough, R.M., Lintern, M.J., Howard, D.L., Kappen, P., Cleverley, J., 2010. The new Maia detector system: methods for high definition trace element imaging of natural material. AIP Conf. Proc. 1221, 9–17.
Sorensen, S.S., Grossman, J.N., Perfit, M.R., 1997. Phengite-hosted LILE enrichment in eclogite and related rocks: implications for fluid-mediated mass transfer in subduction zones and arc magma genesis. J. Petrol. 38, 3–34.
Stöckhert, B., 2002. Stress and deformation in subduction zones: insight from the record of exhumed metamorphic rocks. Geol. Soc. Lond. Spec. Publ. 200, 255–274.
Stöckhert, B., Renner, J., 1998. Rheology of crustal rocks at ultrahigh pressure. In: Hacker, B.R., Liou, J.G. (Eds.), When Continents Collide: Geodynamics and Geochemistry of Ultrahigh-Pressure Rocks. Springer, Netherlands, Dordrecht, pp. 57–95.
Sun, McDonough, W., 1989. Chemical and Isotopic Systematics of Oceanic Basalts: Implications for Mantle Composition and Processes.
Tamblyn, R., Hand, M., Kelsey, D., Anczkiewicz, R., Och, D., 2020a. Subduction and accumulation of lawsonite eclogite and garnet blueschist in eastern Australia. J. Metamorph. Geol. 38, 157–182.
Tamblyn, R., Hand, M., Morrissey, L., Zack, T., Phillips, G., Och, D., 2020b. Resubduction of lawsonite eclogite within a serpentinite-filled subduction channel. Contrib. Mineral. Petrol. 175, 74.
Thompson, J.B., 1955. The thermodynamic basis for the mineral facies concept. Am. J. Sci. 253, 65–103.
Tian, Z.L., Wei, C.J., 2014. Coexistence of garnet blueschist and eclogite in South Tianshan, NW China: dependence of P–T evolution and bulk-rock composition. J. Metamorph. Geol. 32, 743–764.
Tichelaar, B.W., Ruff, L.J., 1993. Depth of seismic coupling along subduction zones. J. Geophys. Res. 98, 2017–2037.
Vho, A., Lanari, P., Rubatto, D., Hermann, J., 2020. Tracing fluid transfers in subduction zones: an integrated thermodynamic and δ18O fractionation modelling approach. Solid Earth 11, 307–328.
Wassmann, S., Stöckhert, B., 2013. Rheology of the plate interface — dissolution precipitation creep in high pressure metamorphic rocks. Tectonophysics 608, 1–29.
Wei, C.J., Clarke, G.L., 2011. Calculated phase equilibria for MORB compositions: a reappraisal of the metamorphic evolution of lawsonite eclogite. J. Metamorph. Geol. 29, 939–952.
Weinberg, R.F., Veveakis, E., Regenauer-Lieb, K., 2015. Compaction-driven melt segregation in migmatites. Geology 43, 471–474.
White, R.W., Powell, R., Halpin, J.A., 2004. Spatially-focussed melt formation in aluminous metapelites from Broken Hill, Australia. J. Metamorph. Geol. 22, 825–845.
White, R.W., Powell, R., Johnson, T.E., 2014. The effect of Mn on mineral stability in metapelites revisited: new *a–x* relations for manganese-bearing minerals. J. Meta. Geol. 32, 809–828.
Whitney, D.L., Evans, B.W., 2010. Abbreviations for names of rock-forming minerals. Am. Mineral. 95, 185–187.
Whitney, D.L., Fornash, K.F., Kang, P., Ghent, E.D., Martin, L., Okay, A.I., Vitale Brovarone, A., 2020. Lawsonite composition and zoning as tracers of subduction processes: a global review. Lithos 370-371, 105636.
Zack, T., Foley, S.F., Rivers, T., 2002. Equilibrium and disequilibrium trace element partitioning in hydrous eclogites (Trescolmen, Central Alps). J. Petrol. 43, 1947–1974.